Optical and Radio Remote Sensing of Space Plasma Turbulence
AFOSR Grant FA9550-05-1-0091

Project Summary

Experiments were conducted at Arecibo, Puerto Rico to investigate naturally-occurring and radio wave-induced ionospheric plasma turbulence. The intriguing phenomena reported here include large-scale turbulence created by tsunami-launched gravity waves [Lee et al., J. Geophys. Res., 2008] and short-scale turbulence generated by VLF waves from the Navy transmitter (code-named NAU) in Puerto Rico [Labno et al., J. Geophys. Res., 2007]. Presented are ionospheric measurements using Arecibo 430 MHz radar supported by data from two ionosondes and GPS satellites. The $M_W = 9.2$ earthquake in Sumatra, Indonesia on December 25, 2004 launched tsunami and then gravity waves first across the Indian, then into the Atlantic and Pacific Oceans, triggering intense ionospheric plasma turbulence over Arecibo. The NAU-generated waves are intense enough to excite lower hybrid waves, which can accelerate electrons continuously along the geomagnetic filed, to cause enhanced plasma lines detected by Arecibo radar in the nighttime ionosphere F region in the presence of spread F events. These energetic streaming electrons, when detected by the Arecibo 430 MHz radar, give rise to enhanced plasma lines with a frequency spectrum of $\sim 3.25 - 4.75$ MHz.

1. Introduction

In the past three years we have been conducting experiments at Arecibo, Puerto Rico to investigate naturally-occurring and radio wave-induced ionospheric plasma turbulence. The intriguing phenomena reported here include large-scale turbulence created by tsunami-launched acoustic gravity waves [Lee et al., 2008] and relatively short-scale turbulence generated by VLF waves injected from ground-based transmitters [Labno et al., 2007]. In the first part of the report we present measurements of ionospheric plasma dynamics conducted at the Arecibo Observatory between 20:00 and 24:00 local time (LT) on December 25 and 26, 2004 using the 430 MHz incoherent scatter radar (ISR) supported by data from two nearby ionosondes and Global Positioning System (GPS) satellites. The ISR detected different ionospheric behaviors during the vertical-transmission periods on the consecutive, magnetically quiet nights. On the night of December 25 the ionosphere descended smoothly and spread F signatures faded. For about two hours on the following evening the bottomside ionosphere rose by ~50 km, inducing plasma irregularities and intense spread F. Alternating cycles of bottom-side plasma rising and falling persisted through the remainder of the experiments. We find that this sinusoidal behavior is a response to gravity waves propagating above Puerto Rico. Nearly simultaneous data from two nearby stations show that GPS signals were modified by variations in total electron content (TEC) indicating the presence of traveling ionospheric disturbances (TIDs). The December 26 experiments were conducted about a day after an $M_W = 9.2$ earthquake launched tsunami waves first across the Indian, then

REPORT DOCUMENTATION PAGE

1. REPORT DATE *(DD-MM-YYYY)*	2. REPORT TYPE	3. DATES COVERED *(From - To)*

4. TITLE AND SUBTITLE

5a. CONTRACT NUMBER

5b. GRANT NUMBER

5c. PROGRAM ELEMENT NUMBER

6. AUTHOR(S)

5d. PROJECT NUMBER

5e. TASK NUMBER

5f. WORK UNIT NUMBER

7. PERFORMING ORGANIZATION NAME(S) AND ADDRESS(ES)

8. PERFORMING ORGANIZATION REPORT NUMBER

9. SPONSORING/MONITORING AGENCY NAME(S) AND ADDRESS(ES)

10. SPONSOR/MONITOR'S ACRONYM(S)

11. SPONSOR/MONITOR'S REPORT NUMBER(S)

12. DISTRIBUTION/AVAILABILITY STATEMENT

13. SUPPLEMENTARY NOTES

14. ABSTRACT

15. SUBJECT TERMS

16. SECURITY CLASSIFICATION OF:			17. LIMITATION OF ABSTRACT	18. NUMBER OF PAGES	19a. NAME OF RESPONSIBLE PERSON
a. REPORT	b. ABSTRACT	c. THIS PAGE			
					19b. TELEPHONE NUMBER *(Include area code)*

INSTRUCTIONS FOR COMPLETING SF 298

1. REPORT DATE. Full publication date, including day, month, if available. Must cite at least the year and be Year 2000 compliant, e.g. 30-06-1998; xx-06-1998; xx-xx-1998.

2. REPORT TYPE. State the type of report, such as final, technical, interim, memorandum, master's thesis, progress, quarterly, research, special, group study, etc.

3. DATES COVERED. Indicate the time during which the work was performed and the report was written, e.g., Jun 1997 - Jun 1998; 1-10 Jun 1996; May - Nov 1998; Nov 1998.

4. TITLE. Enter title and subtitle with volume number and part number, if applicable. On classified documents, enter the title classification in parentheses.

5a. CONTRACT NUMBER. Enter all contract numbers as they appear in the report, e.g. F33615-86-C-5169.

5b. GRANT NUMBER. Enter all grant numbers as they appear in the report, e.g. AFOSR-82-1234.

5c. PROGRAM ELEMENT NUMBER. Enter all program element numbers as they appear in the report, e.g. 61101A.

5d. PROJECT NUMBER. Enter all project numbers as they appear in the report, e.g. 1F665702D1257; ILIR.

5e. TASK NUMBER. Enter all task numbers as they appear in the report, e.g. 05; RF0330201; T4112.

5f. WORK UNIT NUMBER. Enter all work unit numbers as they appear in the report, e.g. 001; AFAPL30480105.

6. AUTHOR(S). Enter name(s) of person(s) responsible for writing the report, performing the research, or credited with the content of the report. The form of entry is the last name, first name, middle initial, and additional qualifiers separated by commas, e.g. Smith, Richard, J, Jr.

7. PERFORMING ORGANIZATION NAME(S) AND ADDRESS(ES). Self-explanatory.

8. PERFORMING ORGANIZATION REPORT NUMBER. Enter all unique alphanumeric report numbers assigned by the performing organization, e.g. BRL-1234; AFWL-TR-85-4017-Vol-21-PT-2.

9. SPONSORING/MONITORING AGENCY NAME(S) AND ADDRESS(ES). Enter the name and address of the organization(s) financially responsible for and monitoring the work.

10. SPONSOR/MONITOR'S ACRONYM(S). Enter, if available, e.g. BRL, ARDEC, NADC.

11. SPONSOR/MONITOR'S REPORT NUMBER(S). Enter report number as assigned by the sponsoring/ monitoring agency, if available, e.g. BRL-TR-829; -215.

12. DISTRIBUTION/AVAILABILITY STATEMENT. Use agency-mandated availability statements to indicate the public availability or distribution limitations of the report. If additional limitations/ restrictions or special markings are indicated, follow agency authorization procedures, e.g. RD/FRD, PROPIN, ITAR, etc. Include copyright information.

13. SUPPLEMENTARY NOTES. Enter information not included elsewhere such as: prepared in cooperation with; translation of; report supersedes; old edition number, etc.

14. ABSTRACT. A brief (approximately 200 words) factual summary of the most significant information.

15. SUBJECT TERMS. Key words or phrases identifying major concepts in the report.

16. SECURITY CLASSIFICATION. Enter security classification in accordance with security classification regulations, e.g. U, C, S, etc. If this form contains classified information, stamp classification level on the top and bottom of this page.

17. LIMITATION OF ABSTRACT. This block must be completed to assign a distribution limitation to the abstract. Enter UU (Unclassified Unlimited) or SAR (Same as Report). An entry in this block is necessary if the abstract is to be limited.

into the Atlantic and Pacific Oceans. The coupling at the tsunami sea-air interface launched gravity waves that propagated for great distances beneath the mesopause. GPS data recorded TEC variation in Asia, Europe, and the Caribbean, suggesting that TIDs were induced on a global scale at the wake of tsunami-launched gravity waves. Energy from imperfectly ducted gravity waves leaked into the ionosphere, partially over Puerto Rico. The wind-velocity field of these gravity waves caused local ionospheric plasma to rise, seeding bottomside irregularities via the generalized Rayleigh-Taylor instability to produce intense large-scale ionospheric plasma turbulence.

In the second part of the report we describe how radio waves transmitted from the Naval transmitter, code-named NAU, in Puerto Rico can affect the ionospheric plasmas over Arecibo. NAU emits radio waves at a power and frequency of 100 kW and 40.75 kHz, respectively. The NAU-generated 40.75 kHz whistle waves are intense enough to excite lower hybrid waves and zero-frequency field-aligned ionospheric irregularities over Arecibo. It is found that NAU is responsible for causing the enhanced plasma lines, detected by the Arecibo 430 MHz radar in the nighttime ionosphere F region, in the presence of spread F events. The lower hybrid waves, generated in a broad range of altitudes at the wake of 40.75 kHz whistler waves, have a single frequency of 40.75 kHz but with a spectrum of wavelengths. They can effectively accelerate electrons continuously along the Earth's magnetic field with energies from a fraction of 1 eV to 10 eV. These energetic streaming electrons, when detected by the Arecibo 430 MHz radar, give rise to enhanced plasma lines with a frequency spectrum of $\sim 3.25 - 4.75$ MHz.

2. Ionospheric Turbulence Created by Tsunami-launched Gravity Waves

The experimental set-up and radar/ionosonde/satellite detections of ionospheric plasma dynamics on two successive nights are briefly described below. In terms of local time at Arecibo, the reported experiments cover the approximate periods 20:00 to 24:00 LT on December 25 and 26, 2004 (00:00 to 04:00 UT on December 26 and 27, 2004). Initially, we transmitted the 430 MHz incoherent scatter radar (ISR) signals while rotating the line feed along the perimeter of a 15° wide cone, in search of turbulent regions in the local ionosphere. After finding active regions, subsequent radar diagnoses were conducted using a stationary line feed that transmitted waves toward local zenith. Figure 1(a) illustrates the general geometry of the experiments on both nights. The primary instruments were the 430 MHz ISR and an ionosonde located at the Arecibo Observatory.

Initially the ISR line feed (i.e., transmitter) tilted 15° from vertical and rotated clockwise from 0° to 360°, and then counter-clockwise from 360° to 0°, bringing the line feed to its original position as illustrated in Figure 1(b). Note that if the line feed pointed toward the northwest, radar waves were emitted toward the southeast. On average 360° rotations took ~15.77 minutes. The radar beam has an angular width of 0.16^o, when transmitting at 430 MHz. The beam-width of the nearby ionosonde is $\sim \pm45^o$ and covers the entire region scanned by the ISR. Ionograms were recorded every 5 minutes. The ionosonde and ISR operated simultaneously to monitor the occurrence of spread F due to bottomside density

irregularities and the evolution of ionospheric distributions in the entire F layer.

(b)

W
270

S 180

0 N

90
E

(a)

50°
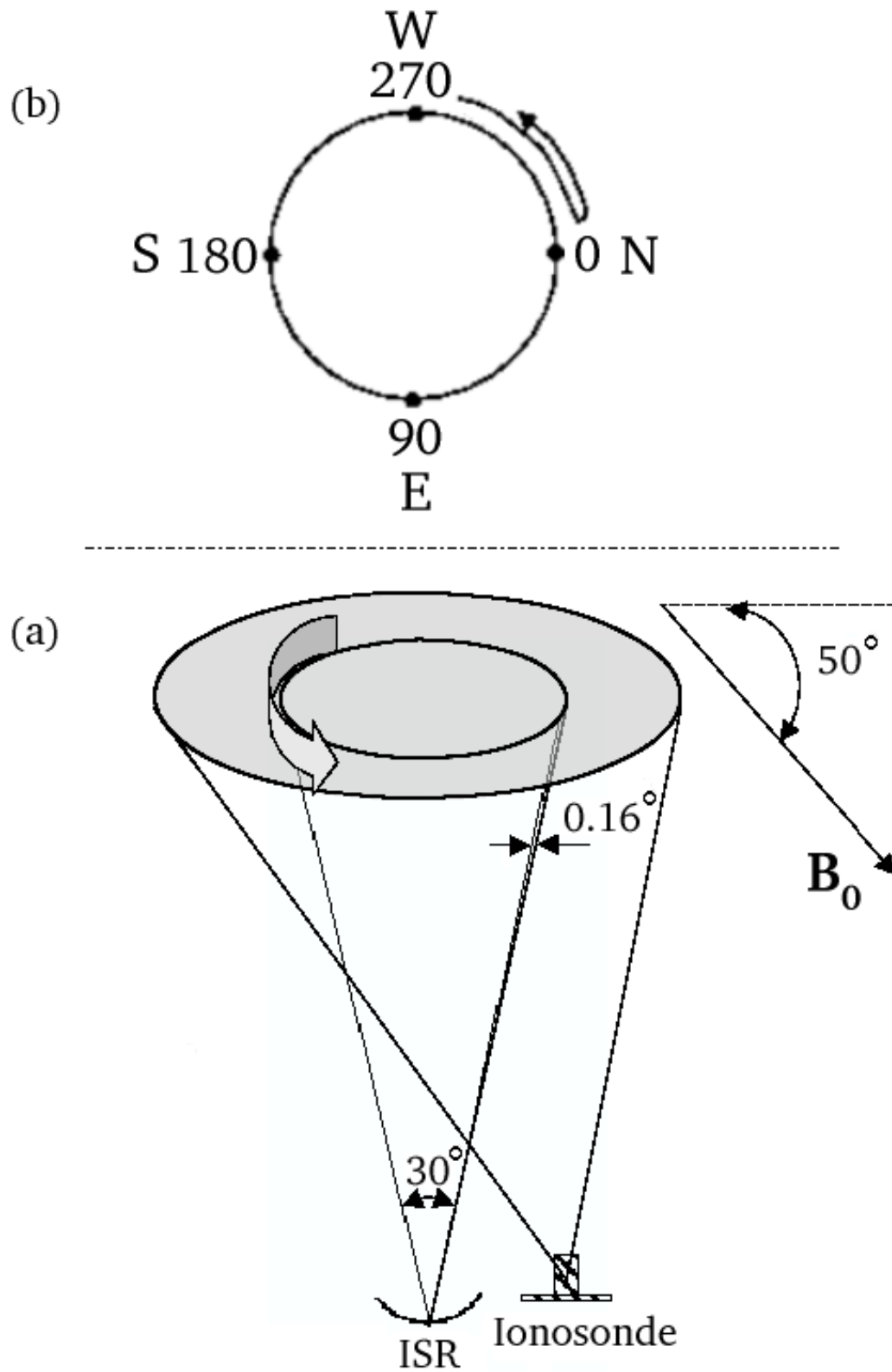
0.16°

B_0

30°

ISR   Ionosonde

Figure 1. (a) Illustration of Arecibo ionosonde and ISR radiating from the rotating, tilted line feed, to diagnose ionospheric plasma turbulence.   (b) Top view of the cone traced by the rotating, tilted line feed of the radiating ISR.

2.1. Arecibo Experiments

December 25, 2004

Figure 2 shows ISR and ionosonde data recorded between 20:00 and 24:00 LT on December 25, 2004. Figure 2(a) shows a range-time-intensity (RTI) plot of backscatter power displayed in a relative intensity format that ranges from 0 to 1. The maximum value of radar backscatter power in a data file is set at an intensity of 1 (corresponding to maximum electron density of 3.0×10^{11} m^{-3}). The color bar to the right of the RTI indicates the intensity of P_b. Dark areas on the RTI plot indicate regions of weak P_b where N_e was low. Seven blank stripes reference radar data gaps that occurred as operational modes changed to take plasma line measurements whose results will be reported elsewhere. During ISR power-mode operations pulses of 52 μs duration were transmitted every 10 ms. They consisted of a 13-baud Barker code with 4 μs bauds, resulting in 600 m range resolution, with an integration of 200 pulses for 2 s time resolution.

Figure 2(b) shows the temporal variation of $\int N_e(t)$ dh, the total electron content (TEC), computed from the height-integrated backscattered power $\int P_b(t)$ dh along the radar beam between 150 and 600 km altitude. Since we expect no heat sources to cause significant change in T_e/T_i at mid-latitudes over this altitude range, $\int P_b(t)$ dh is proportional to $\int N_e(t)$ dh.   Below the local time axis are alternating arrows: $\rightarrow$ and $\leftarrow$ indicating times of clockwise and counter-clockwise radar rotation, respectively. Figure 2(c) contains four ionograms that are representative of conditions in the periods of acquisition.
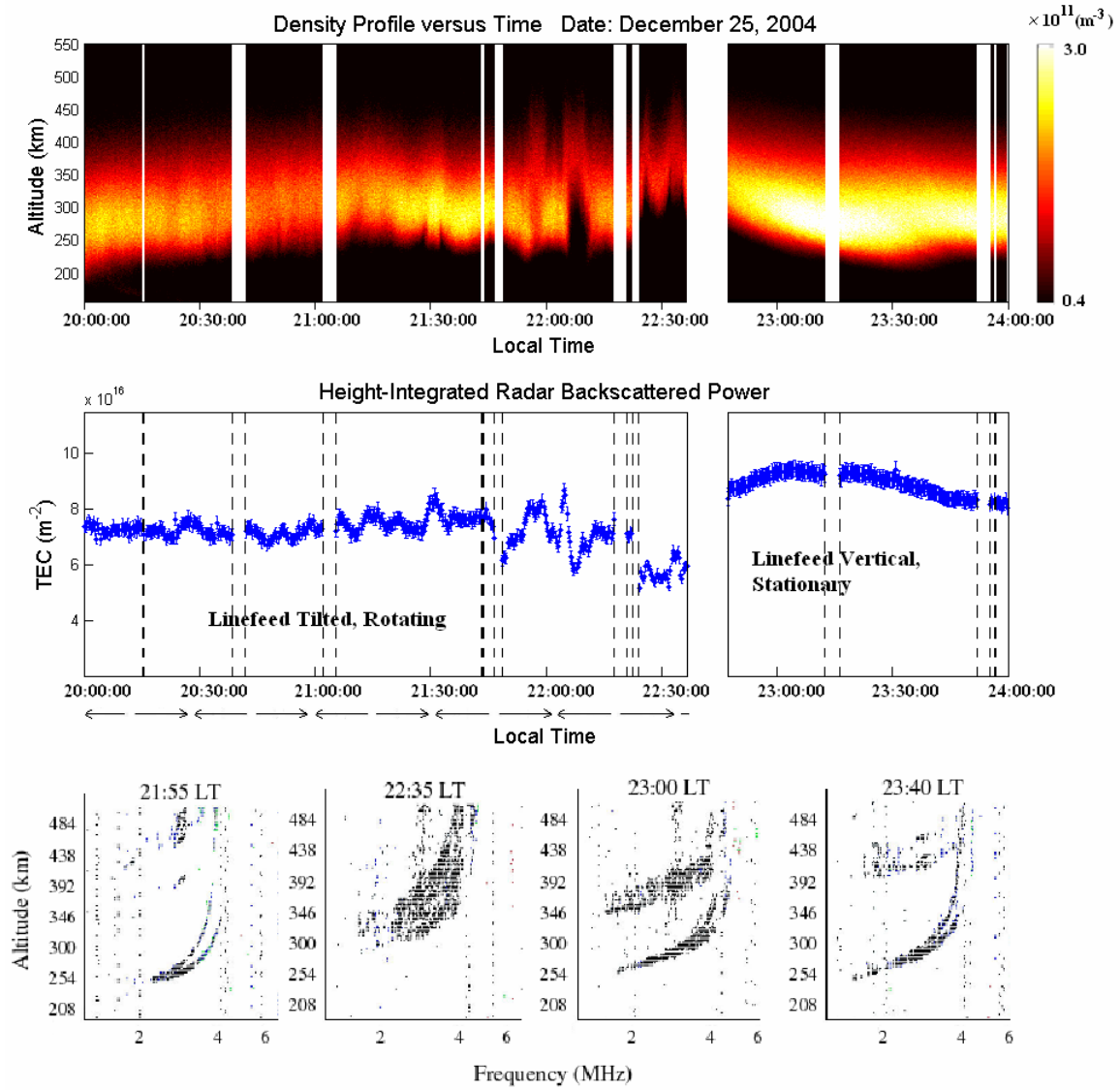
Figure 2. (a) The range-time-intensity (RTI) plot of radar backscatter power recorded on December 25, 2004 from 20:00:00 to 24:00:00 local time (LT). (b) The computed TEC is based on the height-integrated radar backscatter power and plotted as a function of local time. (c) Four representative ionograms recorded during the experiments, to monitor the local ionospheric plasma conditions.

During the initial phase of the rotating line feed operations, 20:00 to 22:05 LT, both the RTI plot and height-integrated backscattered power show relatively quiet ionospheric plasma conditions. Notable plasma density structures and reductions appear in Figure 2 near 22:06 and after 22:25 LT. Spread F echoes accompanied the irregularities (cf. 21:55

LT ionogram). To observe the ionospheric depletion and associated irregularities more closely, we stopped rotating line feed operation at 22:36:42 LT. It took ~15 minutes to bring the ISR line feed to a stationary, vertical position.

Immediately after the stationary radar line feed operations began at 22:47:07 LT, the density reductions/irregularities weakened and spread F echoes faded. From 22:42:29 LT to the end of the experiments at 24:00:00 LT, the radar and ionosonde detected no significant ionospheric turbulence that appeared in Figure 2 following the fall and rise of the F layer.

December 26, 2004

We next discuss Arecibo experimental results obtained between 20:00 and 24:00 LT on December 26 [00:00 to 04:00 UT, December 27], 2004. Figure 3(a) shows three plasma-density profiles recorded between 20:00 and 24:00 local time (LT) on December 26, 2004. Figure 3(b) show the experimental geometry and a schematic representation of a rising plasma depletion indicated by the 3 plasma-density profiles. As on the previous day, the 430 MHz ISR operations began with the line feed tilted and rotating.
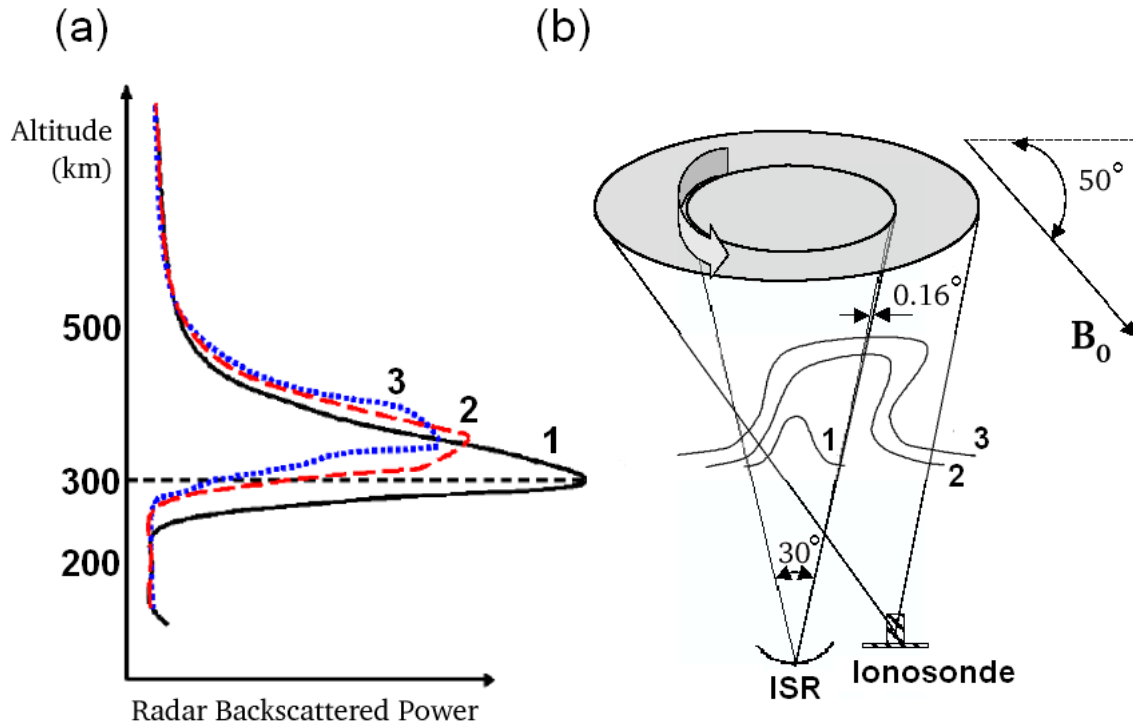

Figure 3. (a) Three ionospheric density profiles recorded on December 26, 2004 at 21:54:12, 22:00:54 and 22:09:17 local time (LT), respectively during the development of

6

ionospheric density depletion and the evolution of a rising plasma bubble. (b) Illustration of Arecibo ionosonde and ISR radiating from the rotating, tilted line feed, to monitor the development of ionospheric plasma turbulence.

The upper panel of Figure 4 shows normalized RTI backscattered powers recorded between 20:00 and 24:00 LT in the same format as Figure 2. Deep ionospheric plasma depletions are prominent features in ionospheric regions probed by the rotating 430 MHz radar beam especially near 20:53:28 LT and 21:27:39 LT. Note that since the radar beam rotation changed from clockwise to counter-clockwise rotation at 21:32:37 LT, the two peaked values in the $\int P_b(t) \, dh$ trace labeled A and B, represent the same plasma structure sampled before and after the reversal. The same ionospheric structure A/B was probed by the rotating radar beam at different times and had changed location due to ionospheric drift, as illustrated in Figure 5. This together with Figure 4 can be used to explain how the rotating radar beam encountered different depleted ionospheric regions as follows.
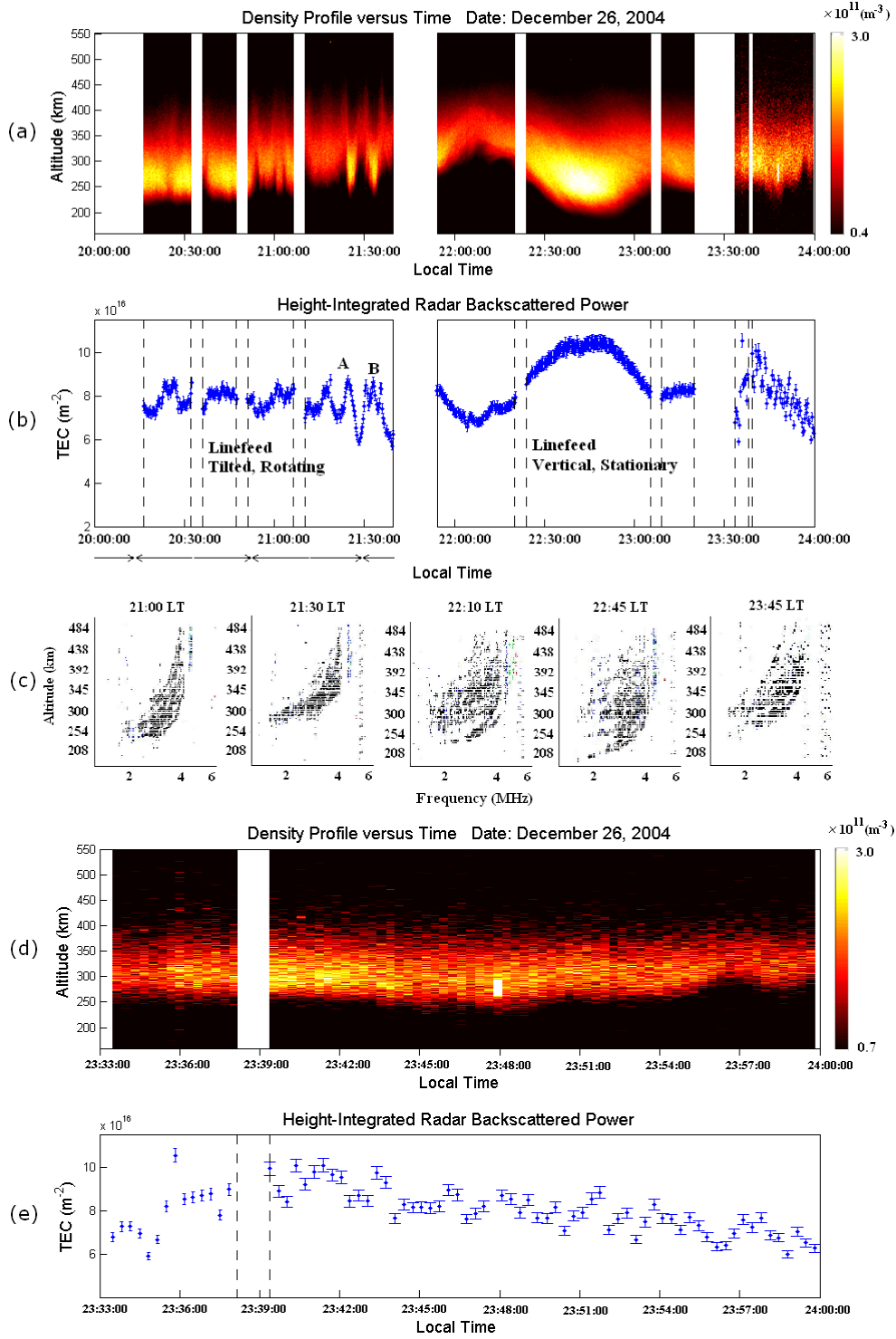
Figure 4. (a) The range-time-intensity (RTI) plot of radar backscatter power recorded on December 26, 2004 from 20:16:21 to 24:00:00 local time (LT). (b) The computed TEC is based on the height-integrated radar backscatter power and plotted as a function of local

time. (c) Five representative ionograms recorded during the experiments that demonstrate the excitation of spread F and naturally occurring ionospheric plasma turbulence.
(d) Enlarged RTI plot recorded from 23:33 to 24:00 LT. (e) The corresponding computed TEC from 23:33 to 24:00 LT.
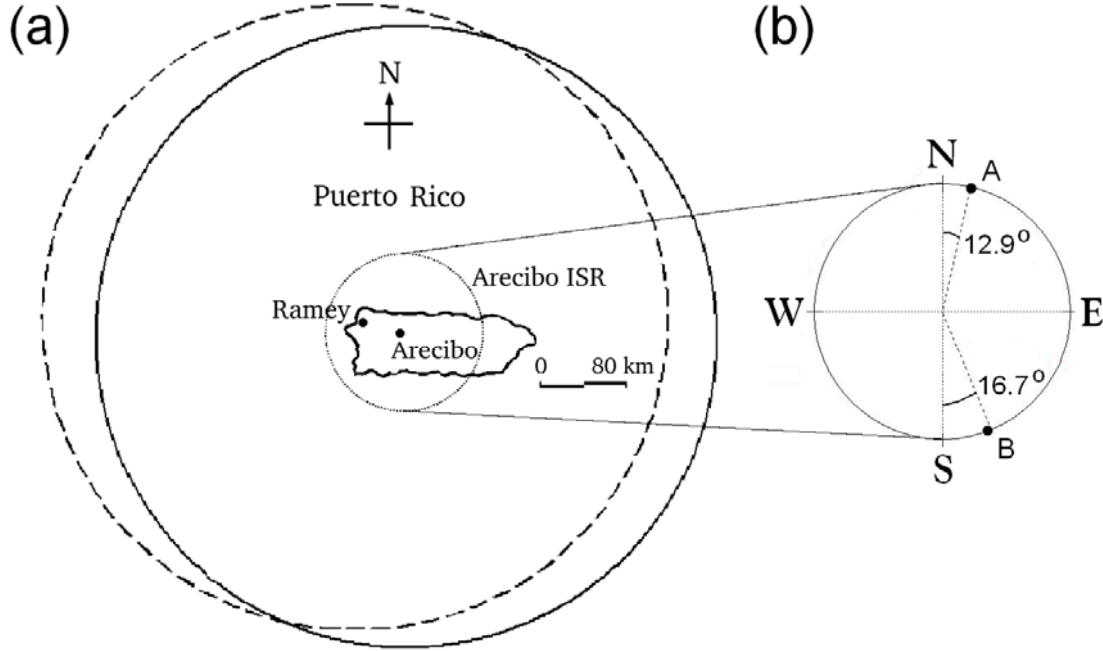

Figure 5. (a) Map of Puerto Rico showing the field of view of Ramey ionosonde (dashed line) and Arecibo ionosonde (solid line), at an altitude of 300 km. The dotted line shows the trace cross-section of Arecibo ISR when the beam is rotating and at a maximum angle from the zenith. (b) Arecibo ISR beam trace cross-section.

The RTI plot and discrete density profiles allow determination of the times when the radar beam intercepted the structures A and B. To within an accuracy of 10 s, the radar beam encountered A and B at 21:25:18 and 21:33:21 LT, respectively. The rotation reversal (radar waves emitted due south) occurred at 21:32:37 LT, 439s after encountering A. The radar beam encountered B 44s after the reversal. Thus, 483s is the approximate time between the radar intercepting A then B, with an uncertainty of 14s. The average radar platform rotation period is 946s. With this information we can calculate the rotation angles of A and B encounters with respect to the south.

Since (439/946) × 360° = 167.1°, the ISR sampled structure A 12.9° away from due north. Likewise the radar crossed structure B (44/946) × 360 = 16.7° away from due south. The uncertainty is ±5°. At the altitude of 300 km and a tilt angle of 15°, the radius of the circle traced by the radar beam traces is ~80 km. Along the east-west direction, A and B are separated by 80 km × (Sin [16.7°] - Sin [12.9°]) = 5.4 km. The estimated east-

9

west component of drift is 5400 m/483 s = 11.2 m/s. This is consistent with the east-west drifts deduced in earlier Arecibo experiments [Lee et al., 1998a]. Because of this small plasma drift, observed dynamic and turbulent ionospheric behavior can be attributed plausibly to the temporal variations of localized ionospheric disturbances detected by the Arecibo radar. The rotating ISR took ~3 minutes to pass across structures A and B, about 19% of the ISR rotation period. A secant drawn as the third side of an isosceles triangle whose two other sides are cone radii separated by an angle of 19% x 360° (= 69°) has a length of 91 km.   Thus, the dense-plasma region is ~ 91 km across. However, since the ISR cone intercepts a narrow cross section of the ionosphere, this must be viewed as a lower limit on the thickness of structure A/B.

Having detected an ionospheric structure, we terminated ISR rotations at 21:39 LT. After brought the line feed to a vertical position, we began stationary operations at 21:54:29 LT. From 21:54 to 22:10 LT the radar observed a significant ionospheric upwelling and density depletion that appears in Figures 4(a) and 4(b) to rise and fall. The three density profiles labeled 1, 2, and 3 in Figure 3(a) were acquired at 21:54:12, 22:00:54 and 22:09:17 LT, respectively. The schematic illustration in Figure 3(b) shows a density depletion developing and moving upward with an apparent velocity of ~100 m/s. Also note in the RTI plot that when the bottomside approached its highest altitude the local plasma became highly structured. Sequentially recorded ionograms support this scenario, showing a large expansion in the altitude range of spread F echoes, while the height of the F peak remained unchanged.   These observations were independently verified in simultaneously recorded ionograms from the nearby Ramey Air Force Base. Figure 5 shows that ionosonde field of views at Arecibo and Ramey nearly overlap.

The RTI plot shows that as the ionosphere descended between 22:12 LT and 22:45 LT bottomside structuring vanished. However, the third and fourth ionograms in Figure 4(c) show that very intense spread F signatures persisted throughout this period. Signs of the bottomside irregularities are evident in the RTI plot especially near 21:10 LT when the F layer was at its highest altitude. The growth rate for bottomside plasma density irregularities should increase at higher altitudes where the effective ion-neutral collision rates are lower. The fact that spread F did not disappear by 22:45 LT suggests that either the plasma descent happened quicker than the recombination time or the irregularities moved to a different part of the sky still observable by the ionosonde, but outside the narrow ISR field of view. The smooth structure of bottomside plasma directly above Arecibo, evident in the RTI plot at 22:45 LT, suggests that the latter interpretation is more probable.

The F layer continued to rise and fall after 22:50 LT with the next peak occurring at ~23:10 LT.   At 23:30 LT power to the ISR was reduced to 1/3 its normal level to maintain transmitter stability. Since the intensity of radar backscattered power was proportionately reduced, RTI recordings from 23:30 to 24:00 LT show diminished temporal and spatial resolution. Figures 4(d) and 4(e) are enlarged plots of the RTI and

10

TEC measured during the ISR reduced-power interval. Both the height of the F layer and TEC manifest persistent, wavelike cycles of rising and falling plasma, albeit with diminished amplitude. Note that the 5th ionogram in Figure 4(c) indicate that intense spread F continued during this interval.

2.2. Tsunami-Induced Gravity Waves and Ionospheric Turbulence

To help quantify the relative intensities of plasma turbulence on the two nights, we developed a Spread F Index (SFI), defined as the ratio of the total received power for an ionogram with spread F to that of a typical ionogram without it. Spread F irregularities produce multiple signal reflections thereby increasing the signal recorded in an ionogram. By definition SFI = 1 when no Spread F is present. Values near 1.5 and $\geq$ 2 indicate Spread F intensities that are light and fully developed, respectively. Figure 6 compares SFI values calculated from ionograms recorded on December 25 and 26 between 20:00 and 24:00 LT. Considerable differences between the two nights are apparent. On December 25 [Figure 6(a)], the maximum SFI was ~3 and lasted for about an hour. On December 26 [Figure 6(b)], the SFI was >3 for nearly 2 hours with a maximum of ~3.5. Clearly, the ionosphere was more disturbed on the 26th than 25th of December.
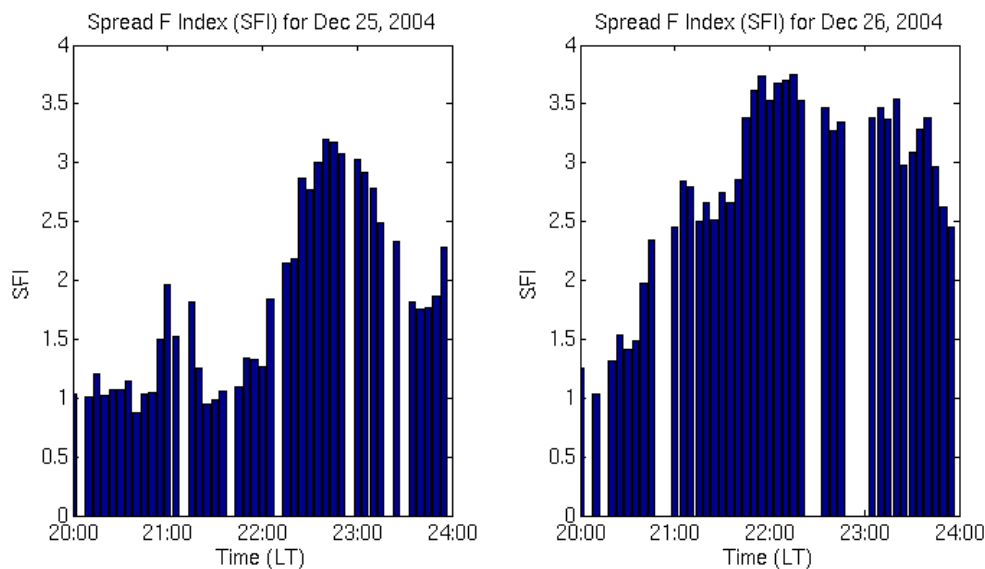

Figure 6. Spread F index (SFI) ionograms recorded by the Arecibo ionosonde on December 25 and December 26, 2004 during 20:00-24:00 LT. Each bar is the SFI for a particular ionogram.

Nicolls and Kelley [2005] reported experimental evidence for GW seeding of ionospheric plasma irregularities at Arecibo. They postulated that the causative GWs were generated by intense magnetic activity at auroral latitudes and then propagated primarily in the meridional direction as a train of traveling ionospheric disturbances (TID). As pointed out in the introduction, geomagnetic conditions were relatively quiet both before and

11

during the period of our experiments. Auroral electrojet indices as well as particle and field measurements from multiple DMSP satellites indicate that geomagnetic activity was low for many hours prior to both ISR experiments. Thus, GWs, in the form of traveling ionospheric disturbances (TID) launched by auroral activity appear unlikely throughout the periods of interest.

Since the observed ionospheric effects were quite unusual and large, it is unlikely that local thunderstorm activity could have caused the observed ionospheric response and plasma depletions. In fact, the National Climatic Data Center (NCDC) website (http://www.ncdc.noaa.gov/oa/climate/research/2004/dec/hazards.html#Storms) claims, "No reports of severe storms were received during December 2004". It is relevant to note that during the summer of 2004 we conducted similar experiments at Arecibo. We observed no significant spread F events at Arecibo Observatory from August 9 through 19. This was true even on the night of 13 August when Hurricane Charlie made landfall on the west coast of Florida at ~ 17:00 and moved off the east coast at about 23:30 LT. Note that this hurricane was nearby but did not pass over Puerto Rico. In contrast, Bishop et al. [2006] reported observations of ionospheric perturbations associated with the passage of Tropical Storm Odette through Puerto Rico. Having the uncertainty of general weather effects in mind, we examine unusual sources that may likely be responsible for the occurrence of marked two sequential events observed on December 26, 2004. That is, a large solitary type of disturbances was associated with the rising/falling ionosphere, subsequently followed by a train of wavelike perturbations with persistent spread F features, as seen in Figure 4.

The experiments of December 26, 2004 started about 23 hours after the large earthquake off the west coast of Sumatra, Indonesia. Stevenson [2005] estimated the speed of the tsunami waves on the open Indian Ocean was ~200 m/s. The dual-frequency altimeter on the JASON satellite measured the tsunami's wavelength and amplitude as ~500 km and 30 to 60 cm, respectively [Wilson, 2005]. We thus estimate a wave period of ~42 min. This agrees with wave periods between 20 and 50 minutes shown in Figure 3 of Titov et al. [2005].

Artru et al. [2005a] showed that after the 2001 seismic event tsunami-induced GWs, with typical periods of ~30 minutes, had vertical and horizontal components of velocity near 50 and 200 m/s, respectively. The tsunami-induced GWs propagated from Peru to Japan. The estimated vertical speed suggests that a GW disturbance would take about 2.5 hours after launch to reach ionospheric altitudes. TEC structures appeared 22 hours after the earthquake in the ionosphere above Japan at about the same time that tsunami waves reached its shores.

Garcia et al. [2005], Lognonné et al. [2006], Komjathy et. al. [2006], Liu et al. [2006], Hao et al. [2006], DasGupta et al. [2006], Lognonné et al. [2006], and Occhipinti et al. [2006], respectively, have offered ground and space-based evidence that related ionospheric disturbances occurred after the Sumatra earthquake. It is thus interesting to

speculate that perhaps gravity waves launched by the Sumatra tsunami were responsible for ionospheric disturbances observed over Arecibo. We consider two possible scenarios, represented schematically in Figure 7.

In the first scenario, tsunami-induced GWs due to sea-air interactions (i.e., forced gravity waves) or interactions with coasts [Artru et al., 2005b] would be launched close to the seismic epicenter and propagate along the great circle path between Sumatra (95.78^o E, 3.3^o N) and Puerto Rico (66°W, 18.5^o N). A signal propagating with a horizontal speed of 200 m/s would traverse a path length of 18,000 km in ~25 hours. Encouragingly, this purely kinematic estimate predicts that such a gravity-wave signal to Arecibo at about the right time, when we saw the solitary type of TID in the rising/falling ionosphere. As illustrated in Figure 7 a tsunami-induced traveling ionospheric disturbance (TID) would propagate toward the southwest over Arecibo.
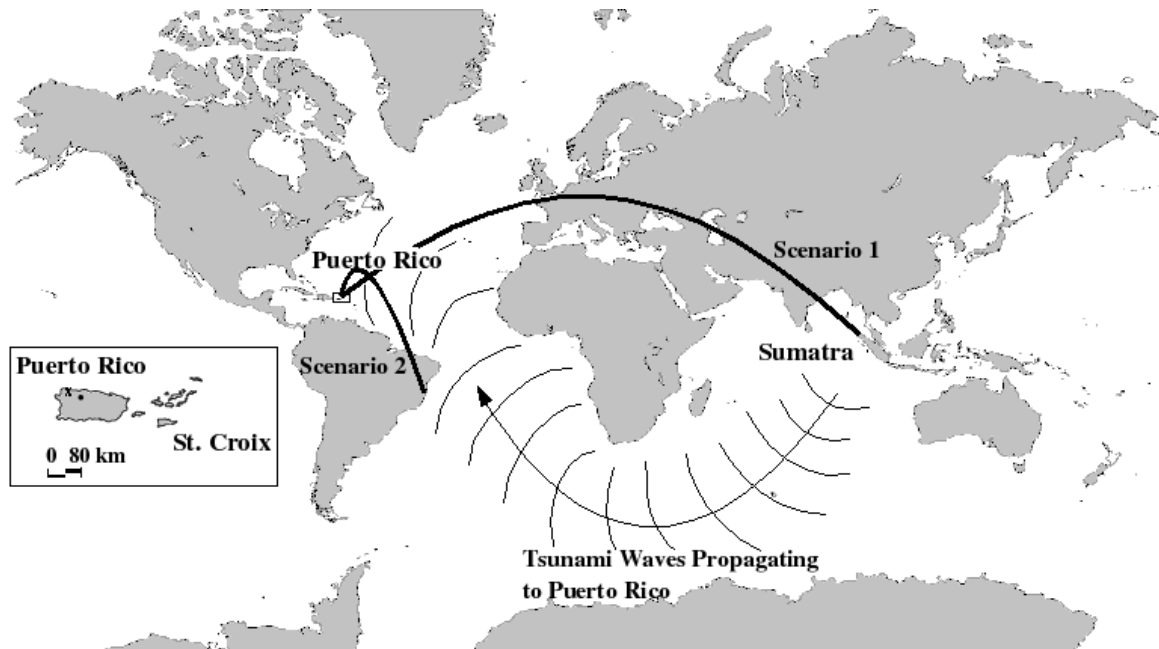

Figure 7. Mercator projection of gravity-wave propagation paths illustrating Scenario 1: along a great circle between northern Sumatra and Puerto Rico and Scenario 2: from moving tsunamis toward Puerto Rico.

Indeed GWs with horizontal speeds of ~200 m/s can propagate over long distances through the lower atmosphere in two Lamb modes that Francis [1973] referred to as L0 and L1. At the wave frequencies and phase speeds of interest the L0 and L1 propagate as "imperfectly" ducted modes (Figure 4 of Francis [1973]) that can circumvent the globe, usually at sub-mesopause altitudes. He also pointed out that horizontal speeds >300 m/s are required for gravity waves to maintain long-range ducting in the ionosphere. While

13

these considerations of gravity-wave dynamics seem to rule out a scenario 1 explanation, care must be exercised before reaching this conclusion. Faced with the fact that imperfectly ducted gravity waves had been observed to reach the ionospheric heights, Hines [1960] (Figure 8) and Hines [1965] (Figure 11) indicated that through not yet understood mechanisms GW energy intermittently finds transmission paths. We note that the modeling by Francis [1973] assumed rather uniform propagation conditions that are not always satisfied in the upper atmosphere. In fact, the tsunami-generated gravity waves that Artru et al. [2005a and 2005b] postulated to be the sources of observed TEC disturbances, have similar L1 mode characteristics to those reported here. There is one significant difference between the two cases. The tsunami-generated gravity waves propagate over open water between Peru and Japan [Artru et al., 2005a]. Large landmasses stand between Sumatra and Puerto Rico.

Following Hines [1960; 1965] we suggest that imperfectly ducted L1 waves mostly propagated for great distances below the mesopause. Occasionally, however, GW energy was subject to partial scattering into the ionosphere. At ionospheric altitudes these waves still propagated but experienced energy losses. The e-fold length for L1 wave attenuation in the ionosphere is ~500 km. Thus, in principle an L1 wave, propagating as a TID could be responsible for the phenomenology observed at Arecibo on December 26, 2004.

Titov et al. [2005] combined tide-gauge and satellite-altimetry data with numerical modeling to demonstrate that surface disturbances propagated beyond the Indian Ocean. Guided by sub-surface mid ocean ridges and continental shelves seismic generated tsunamis were observed to span the Atlantic and Pacific. Somewhat counter intuitively, wave amplitudes measured far from Sumatra in the Atlantic and Pacific were greater than some observed fairly near the epicenter. Tide-gauge data indicate that after intense first-disturbance tsunami waves, amplitudes often weakened rapidly. Modeling results of Titov and coworkers suggest a second scenario (Figure 7), in which gravity waves responsible for the ionospheric behavior observed at Arecibo as a train of TIDs were generated relatively close to Puerto Rico, as tsunami waves propagated northward toward the coast of Brazil. According to Titov et al. [2005] these TIDs should reach Arecibo ~27 hours after the initial seismic event. This model brings our interpretation of Arecibo measurements into closer alignment with the explanation of Artru et al. [2005a] for TEC disturbances over Japan ~ 22 hours after a tsunami-generating seismic event off the coast of Peru in 2001, and with the recent computer modeling by Occhipinti et al. [2006] for the 2004 Sumatra event. In the case considered by Artru et al. [2005a], cross-Pacific tsunami waves and ionospheric gravity waves arrived in Japan nearly simultaneously. In the second scenario, TID (forced gravity waves) generated by tsunami waves would propagate in the northwest direction over Arecibo.

Figures 4 and 8 offer supporting evidence for the presence of wave train propagating over Arecibo between 21:54:29 and 24:00:00 LT on December 26, 2004 during the stationary radar operations. Figures 8(a) and 8(b) shows contours of constant backscattered power

14

and altitude versus local time and peak plasma density as a function of local time, respectively. The upper display [Figure 8(a)] configures the RTI plot to illustrate more explicitly the upward/downward motions of electron-density isocontours. The lower panel [Figure 8(b)] shows the temporal variations of the NmF2 layer.
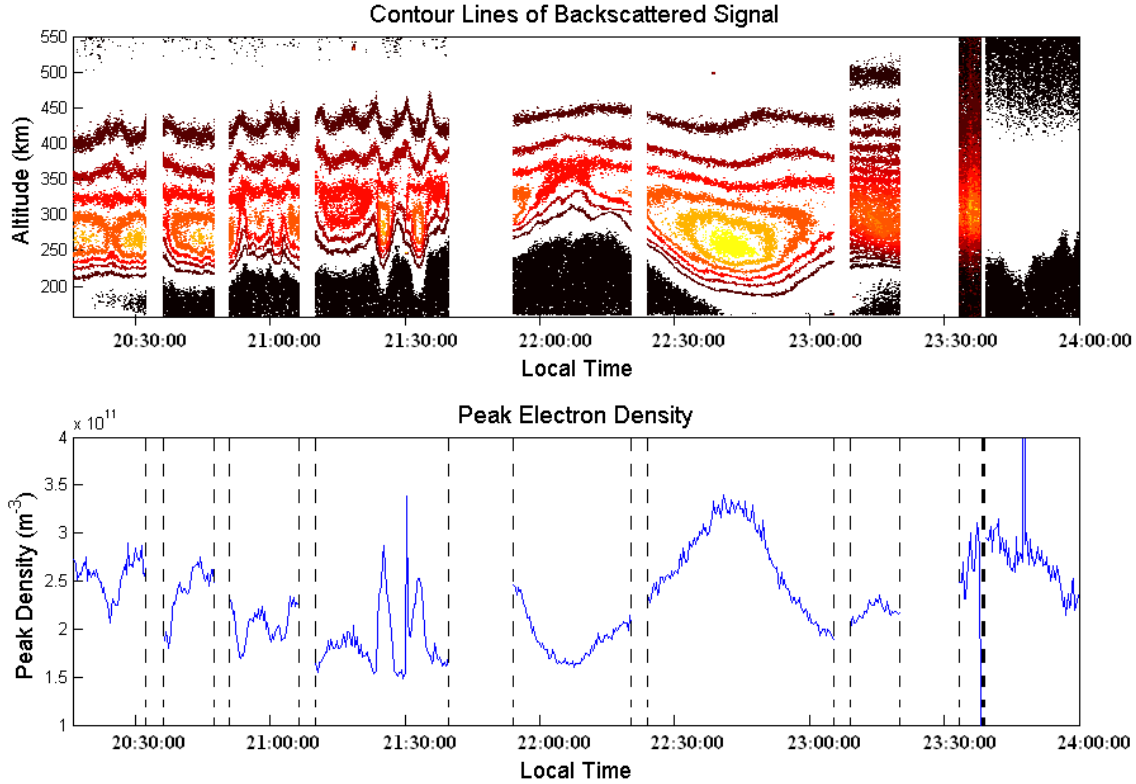

Figure 8. (a) Contours of constant backscattered power plotted on a range-versus-time grid. (b) Temporal variations of the maximum backscattered power are derived from discrete power profiles. This quantity is proportional to peak electron density NmF2.

The second scenario in which causative gravity waves were generated by nearby tsunami waves is consistent with the wavelike up/down sequence of F layer density observed after 23:33 LT, in the enlarged plots of Figures 4(a) and 4(d). The observed up/down motions of the F layer suggest that gravity waves were the causative agent. The timing of these events and the lack of other apparent agents (auroral activity and severe tropospheric disturbances) make it plausible that they were generated by tsunami waves. Presented below are GPS measurements that indicate that TIDs were active in the vicinity of Arecibo and support both scenarios used to explain the ISR data acquired on December 26, 2004.

15

2.3. GPS Measurements

We examined all available GPS measurements of TEC acquired over the December 25 – 27, 2004 time period to determine when and where TID signatures occurred. Specifically, we focused on those GPS data that indicate the presence or absence of TIDs near Puerto Rico moving (1) in the southwest direction between 22:20 and 23:20 LT on December 26 (02:20 to 03:20 UT, December 27) and (2) in the northwest direction between 23:33 and 24:00 LT on December 26 (03:33 to 4:00 UT, December 27), as predicted for Scenarios 1 and 2, respectively. Timely detection of such TID activity would add plausibility that the disturbances detected by the ISR over Arecibo were related to the Sumatra tsunamis.

Vertical TEC (VTEC) values were estimated over the globe using the MIT Haystack Observatory's Madrigal database to compute the TEC perturbation (TECP). Where ever data are available the Madrigal database provides VTEC estimates in 1° latitude by 1° longitude bins every 5 minutes. The data are processed routinely by the MIT Automated Processing of GPS (MAPGPS) software package. Over 200 days of TEC data are currently available on-line at http://www.haystack.mit.edu. Rideout and Coster [2006] and Nicolls et al. [2004] describe the processing algorithms and the procedures used to compute TECP, respectively. VTEC data are detrended by subtracting 2-hour running averages in each latitude-longitude bin to produce TECP maps. This method provides perturbation magnitudes to within a fraction of a TEC unit.

Separate runs of the MAPGPS program were also made to obtain the slant TEC (STEC) values from the different satellites in view of GPS receivers located near Arecibo. The two GPS receiver sites of interest in this study are the PUR2 site at Isabella, Puerto Rico (18.462^o N, 67.067^o W) and CRO1 at Christiansted, St. Croix (17.7569^o N, 64.584^o W). As indicated in Figure 7 they are separated by ~225 km. The presence of TID structures can be studied by comparing STEC values measured simultaneously at the different sites. Also, by computing differences in TEC observed from the same satellite at different receiver sites, perturbations in the TEC can be measured using data from several satellites.

Figure 9 contains six snapshots excerpted and generated in every 15 minutes from a global movie of GPS/TID data acquired between 01:00 and 17:30 UT on December 26, 2004 (21:00 LT, December 25 – 13:30 LT, December 26, 2004), superposed onto global or regional maps. We divide data of the interval into three periods characterizing the ionosphere: (I): post-earthquake but prior to detections of TID activity, (II): initial widespread and sustained tsunami-induced TIDs, and (III) a late TID signature observed off the Atlantic coast of Spain. These snapshots provide evidence that tsunami indeed launched GWs that propagated away from Sumatra and, as elaborated below, appear responsible for a TID observed over the eastern Atlantic Ocean propagating toward Puerto Rico.
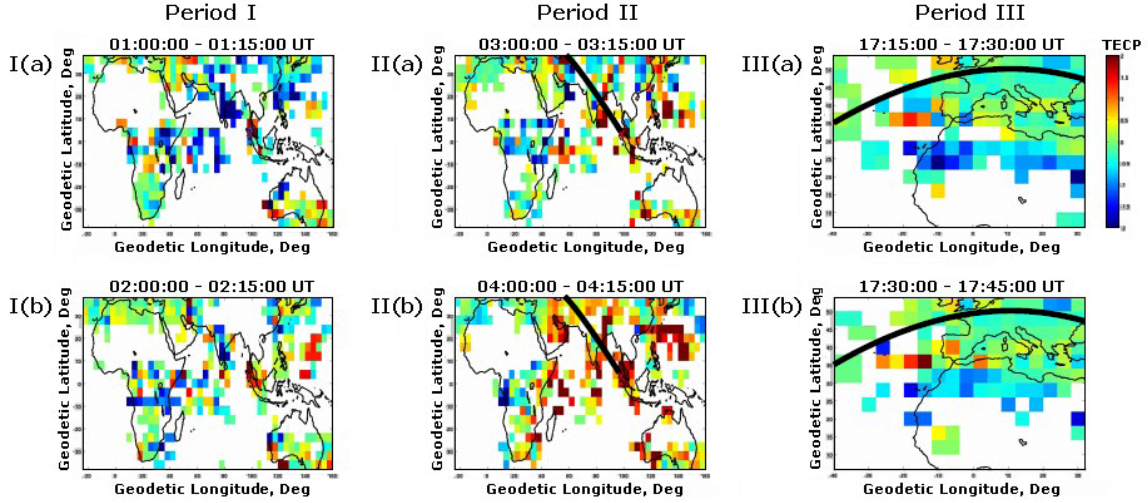
16

Figure 9. Six panels of snapshots selected from a GPS TID movie clip covering the 01:00 – 17:30 UT interval on December 26 (21:00 LT, December 25 – 13:30 LT, December 26), which has 3 periods of time to notice: (I): post-earthquake but prior to detections of TID activity, (II): initial widespread and sustained tsunami-induced TIDs, and (III) a late TID signature observed off the Atlantic coast of Spain. Black lines superposed on data from Periods II and III represent segments of the great circle connecting Sumatra and Puerto Rico.

Period I:

Figures 9-I(a) [01:00-01:15 UT] and 9-I(b) [02:00-02:15 UT] show TEC distributions acquired in the Asian-African longitude sector after the earthquake, but before any tsunami-launched GWs could propagate to ionospheric altitudes. Recall that following Artru et al. [2005a] we approximated the upward propagation time to be about 2.5 hours". Attention is directed to two aspects of the TEC maps. First the coverage has significant gap, especially over broad oceans spans. Second, no striking organization appears in TEC distributions that suggest no significant TID activity occurring during this early, post-earthquake interval.

Period II:

The TEC map in Figure 9-II(a) [03:00-0315 UT] shows the beginning of intense TEC bunching that spans longitudes from central Asia to the eastern Pacific Ocean. But the TEC map in Figure 9-II(b) for 04:00-04:15 UT shows that (1) the disturbance had spread to the African and Middle East longitudes, and (2) disturbances in the Asian-Pacific sector had expanded. Clearly large TECP enhancements (i.e., TIDs) appeared about 2 to

17

2.5 hours after the tsunami initiated. This initial ionospheric response to the tsunami-launched GWs (forced gravity waves) is consistent with the propagation-delay estimates of Artru et al. [2005a]. These forced gravity waves had propagation speeds comparable to tsunami speed of ~ 200 m/s. The TEC maps suggest that GW energy radiated away from a source near Sumatra. Note that TID activity detected in the Middle East provides assurance that GW energy also radiated in the direction of great circles connecting Sumatra and Puerto Rico.

In addition to forced gravity waves generated by tsunamis, there were fast moving acoustic waves induced by Rayleigh seismic waves [e.g., Ducic et al., 2003; Artru et al., 2004; Lognonné et al., 2006; Occhipinti, 2006]. The theory of generating ionospheric seismic signals is discussed in, for example, Lognonné et al. [1998] and Artru et al. [2001]. It can be seen from Figures 9-II(a) and 9-II(b) that TECP related to Rayleigh seismic waves covered a large horizontal extent from Africa to Asian-Pacific. This indicated that these waves had large horizontal propagation speeds of, at least, ~ 700 m/s, reaching southern Africa at 04:00 from Sumatra. The real speed is expected to be close to the Rayleigh seismic waves 3.6 km/s , if we take into account the time for the induced acoustic signals to reach the ionosphere [Artru et al., 2004]. Ionospheric signals (TECP) related to Rayleigh seismic waves were detected in Asia in the event of Sumatra earthquake [Liu et al., 2006a; Hao et al., 2006b] and in Europe [Occhipinti., 2006]. If Rayleigh seismic signals had reached Puerto Rico, they would have caused TECP over Arecibo a few hours after the Sumatra earthquake on the late night of December 25. However, no significant TECP and spread F activities were seen during our experiments on December 25. In other words, there was no evidence that Rayleigh seismic signals could propagate far from the epicenter of Sumatra earthquake to reach Puerto Rico. This is probably due to the absence of a horizontal component of displacements in the acoustic waves driven by the Rayleigh seismic waves

Period III:

After about an hour earthquake-related TID activity seemed to vanish from the global map for many hours. In carefully examining the two-day movie we noticed that signs of TID activity reappeared about 13 hours later in the eastern Atlantic to the west of Spain. The ionospheric signatures of TID activity are shown in the regional maps of Figures 9-III(a) [17:15-17:30 UT] and 9-III(b) [17:30-17:45 UT]. The TID and causal GWs were propagating to the west. Due to lack of GPS coverage in the mid-Atlantic it is not possible to follow their propagation after 18:00 UT.

Our attention was first directed to these disturbances because of their proximity to the great circle between Sumatra and Puerto Rico. Second, the TIDs were detected between 16 and 17 hours after the Sumatra earthquake. The travel time for a 200 m/s signal to propagate from Sumatra to observed TID locations off coast of Spain is about 62% of the 25 hours to when the Arecibo ISR detected TEC and height variations in the ionosphere.

Coincidentally, it is also about 62% of the distance between the two points.

Why might an L1 wave suddenly leak energy into the ionosphere near the Spanish coast? GPS detected its effects between 17:00 and 18:00 UT, near the dusk meridian. Although the wave propagated to the west in the corotating frame, it actually moved to the east in inertial coordinates. The corotation speed in m/s is about 465 Sin λ, where λ represents the instantaneous latitude along a ray propagation path. At the dusk meridian the solar zenith angle varies most rapidly. This is probably reflected in altered characteristics of the sub-mesopause duct in which most of the GW energy propagates.

Taken together we believe that GPS measurements of Period III provide strong, albeit circumstantial, evidence in support of our proposed Scenario 1 for tsunami-generated GWs causing the ionospheric disturbance detected by the Arecibo ISR. We now turn to consider GPS-based evidence for TID activity in the Caribbean sector near the time of our Arecibo measurements.

Figures 10-12 present GPS data acquired between 20:00 LT, December 26 to 02:00 LT, December 27 (00:00 and 06:00 UT on December 27) that indeed indicate the presence of TIDs over the Arecibo Observatory. Figure 10 shows line-of-sight TEC (equivalent to STEC) from a single GPS satellite (satellite navigation vehicle, SNV, #10) as measured by the PUR2 and the CRO1 receivers. The overall shapes of the TEC-versus-UT curves determined at the two sites are related to the satellite's orbit. In this section of the pass, the satellite was moving toward lower elevations. Thus, the receivers were gradually observing longer and longer ionospheric path lengths. For clarity, an offset in TEC was added to separate the two curves and illustrate differences in the fine-scale structure of the observed TEC. Figure 11 shows the differential STEC (DTEC) between three different GPS satellites (SNV #10, #26, and #29) from 20:00 LT on December 26 to 02:00 LT on December 27, 2004. DTEC features at the two sites are repeatable for all three satellites. Satellites #26 and #29 were moving in similar orbits and were being tracked at fairly high elevations and at azimuths between 0° and 50°. Therefore it is not surprising that observed features are similar. In contrast, magnitudes of all TEC perturbations examined on the previous day from 20:00 LT, December 25 to 02:00 LT, December 26 were small, in the few TEC unit range.
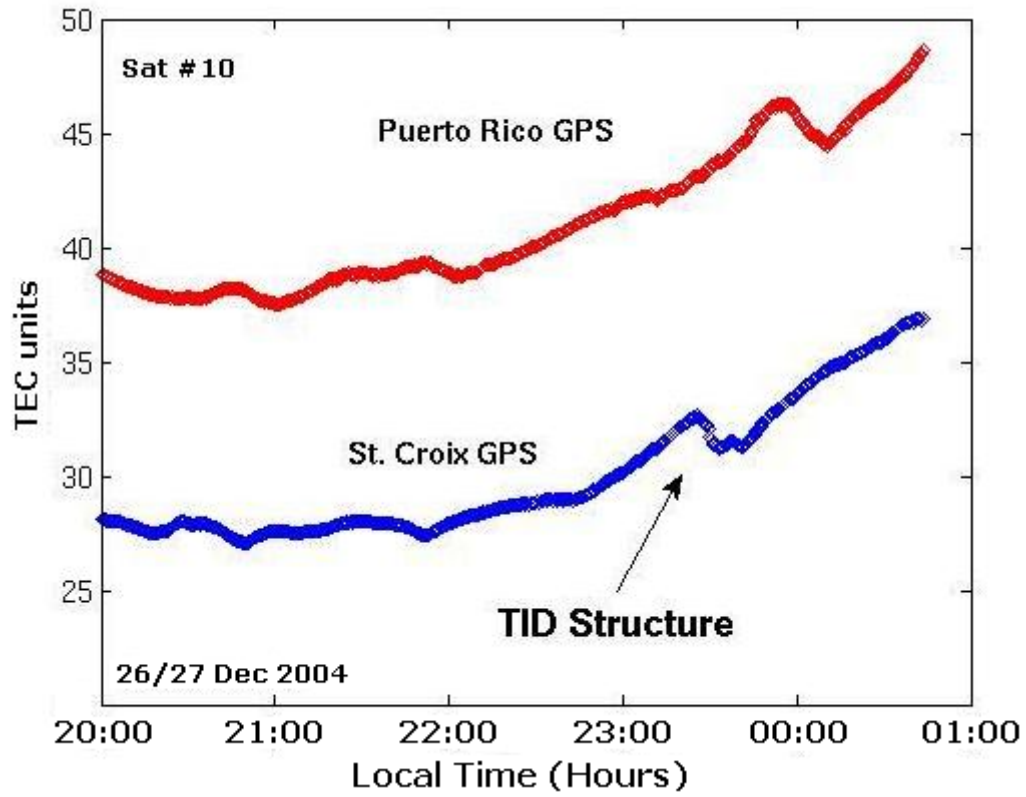
19

Figure 10. The line of sight TEC data from a single GPS satellite (#10) measured by GPS receivers located in Puerto Rico and in St. Croix at a separation of ~225 km.
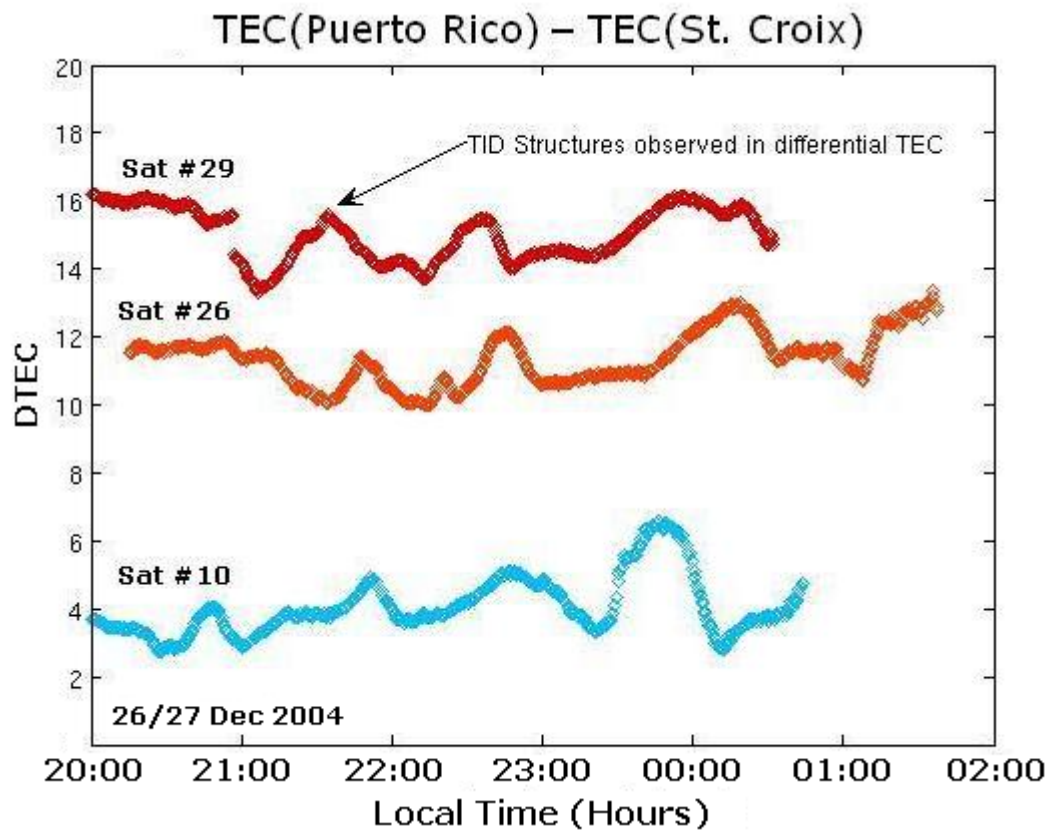
Figure 11. The differential STEC (DTEC) between three different GPS satellites (no. 10, 26, and 29) are shown for the time period 20:00-02:00 LT on December 26-27 2004.
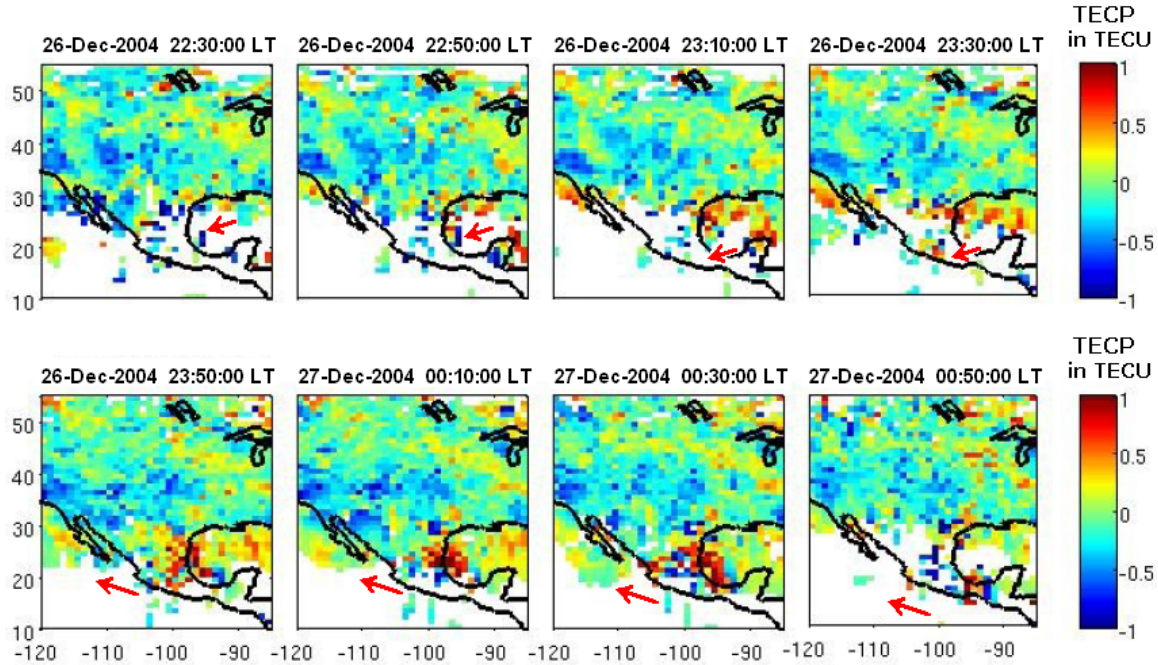
Figure 12. Eight TECP maps selected from TEC movie clip to demonstrate TID activity over the Caribbean Sea and the Gulf of Mexico to the west of Puerto Rico. Arrows indicate TID propagation directions toward the southwest from 22:30 to 23:30 LT on December 26 and northwest from 23:50 LT, December 26 to 00:50 LT, December 27 consistent predictions of Scenarios 1 and 2, respectively.

It is important to note that small TEC anomalies appear in both the PUR2 and CRO1 data sets. The largest anomaly, marked as a TID structure in Figure 10, manifests an ~3 TEC unit change. This TID feature was seen first by CRO1 at ~23:30 LT on December 26, and by PUR2 at ~00:00 LT on December 27. During this period, the GPS satellite was being observed at a fairly low elevation angles and at azimuths between 60° and 120°. Plots displayed in Figures 10 and 11 together with Figure 9 demonstrate that from 22:50 LT on December 26 to 00:50 LT on December 27 the solitary type of TEC perturbations moved toward the southwest over the Caribbean Sea and Gulf of Mexico. These GPS data verify the independent measurements by Arecibo radar of the similar structure, having ~ 3 TEC unit change and moving toward the southwest direction (Figure 7). These results show that the same ionospheric disturbances were detected by the ISR and GPS sensors, albeit at different locations and times. They are again consistent with Scenario 1 of ionospheric turbulence, triggered by tsunami-launched gravity waves after traveling long distances from Sumatra to Puerto Rico.

Scenario 2 turbulence in the ionosphere over Arecibo was associated with weaker TEC

variations seen in the RTI plots of Figures 4(a) and 4(d), recorded from 23:33 to 24:00 LT on December 26 (03:33 – 4:00 UT on December 27). We believe that they too were triggered by tsunami-launched gravity waves that had propagated into the Atlantic Ocean, (Figure 7). This scenario is supported by the TECP maps near Puerto Rico displayed in Figure 12, whose 8 panels were selected from the TID movie clip, covering the 22:30 LT, December 26 – 00:50 LT, December 27 (02:30 – 04:50 UT interval on December 27). These TECP maps cover the western Caribbean and Gulf of Mexico, in as close proximity to Puerto Rico as allowed by the prevailing distributions of GPS satellites and ground receivers. Signals reaching the PUR2 and the CRO1 receivers did not come from zenith, leaving blank spots on the maps. The vertical/ horizontal axes indicate latitude/longitude. We see that between 22:30 an 23:30 LT on December 26 (upper four panels) TIDs drifted toward the southwest, as indicated by arrows. By contrast, arrows in the lower four panels show TIDs moving toward the northwest between 23:50 LT on December 26 to 00:50 LT on December 27. The upper/lower sets of panels are consistent with predictions of Scenarios 1/2 for the Sumatra-tsunami having triggered the ionospheric turbulence detected by Arecibo radar and ionosonde. The full TECP movie for Figures 9-12 is available for examination at http://web.mit.edu/coqui/TEC-movie/.

2.4. Discussions and Conclusions

Gravity waves have embedded wind structures that through ion-neutral collisions move ionospheric plasma along and across magnetic field lines. This neutral-plasma coupling can be elucidated in terms of the following ion momentum equation:

$$n_i m_i (\partial/\partial t + V_i \cdot \nabla) V_i = -\nabla P_i + n_i m_i g + n_i e(E + V_i \times B) - n_i m_i \nu_{in}(V_i - U_n) \qquad (2)$$

where n_i, m_i, g, e, V_i, P_i, ν_{in}, U_n, E and B denote ion density, ion mass, gravity, electric charge, ion velocity, ion pressure, ion-neutral collision frequency, neutral wind velocity, and the local electric and magnetic fields, respectively. As mentioned above, Figure 7 indicates that Scenario 1 gravity waves should propagate toward the southwest over Puerto Rico. If a Cartesian system of coordinates is adopted with its x, y, and z axes taken along west, south, and vertical directions, respectively. Then, we set $U_n = \hat{x} U_{nx} + \hat{y} U_{ny}$ where xU_{nx} and yU_{ny} are neutral wind velocity components perpendicular and parallel to the meridional plane, respectively.

In the rest frame of the plasma, neutral winds provide an induced electric field $E_G \sim \hat{y} U_{ny} B(\nu_{in}/\Omega_i)$ where Ω_i is the ion cyclotron frequency and B is the total strength of Earth's magnetic field. This perturbation neutral wind field creates $E_G \times B$ plasma drifts across the magnetic field. Meanwhile the neutral wind velocity moves plasma along the magnetic field at about the same velocity. Consequently, large-scale plasma redistribution (interchange) is caused by the perturbation neutral velocity due to gravity

waves, as seen in the RTI plot of December 26, 2004 (Figures 4 and 8).   From Equation (2), one can estimate that the neutral wind velocity U_n is sufficient to produce the observed effects, if $U_n > g/\nu_{in}$, about a few meters per second in the nighttime F region.

The density depletion seen in Figure 4 is associated with a change of more than 3 TEC units, confirmed by GPS measurements. This is significantly larger than the $\sim \pm 1$ TEC unit effect that Artru et al. [2005a] attributed to a tsunami-induced gravity wave crossing the Pacific Ocean. Furthermore, in the nighttime mid-latitude ionosphere there are no sources of new plasma to "refill" depleted flux tubes. The observed "rising" depleted flux tubes must be viewed as the consequence of an interchange instability that allowed plasma rich and plasma poor flux tubes to sit side by side. The RTI/TEC and ionograms in Figure 4 show that while the ionosphere rose in altitude, spread F intensified. Since effective ion-neutral collision rates decrease with altitude, the Rayleigh-Taylor growth rate accelerates. After the height of the ionosphere above Arecibo decreased, spread F did not vanish. This reflects two effects:(1) new irregularities formed elsewhere as the gravity wave propagated across the ionosonde field-of-view, and (2) cross-field diffusion takes several tens of minutes to erode large-scale irregularities. Many measurements of gravity waves have been made over the past decade at the Arecibo Observatory, using incoherent scatter power profiles [e.g., Djuth et al, 1997; Djuth et al., 2004; Nicolls and Kelley, 2005 and references therein]. Although the source(s) of these gravity waves over Arecibo were not discussed by Djuth et al. [1997, 2004], auroral- and tsunami-related events were identified in Nicolls and Kelley [2005] and the present paper, respectively.

In summary, the rotating radar beam successfully intercepted active ionospheric regions on successive nights. Subsequent stationary/vertical transmissions, designed to monitor the detailed development of ionospheric irregularities detected very different behaviors on these nights. The different radar responses verified by GPS measurements of regional TEC suggest that on December 26 gravity waves passed Puerto Rico causing plasma in the ISR field-of-view to rise and fall. Consistent with growth rates for the generalized Rayleigh-Taylor instability, RTI measurements showed bottomside irregularities forming as the local ionosphere approached its maximum height. The continuance of strong spread F signatures after plasma seen by the ISR descended suggests that new irregularities were created as the wave continued to propagate within the much broader ionosonde field of view. In the absence of other obvious geophysical sources responsible for observed large-scale "solitary type" of gravity waves and, then subsequently, a train of gravity waves, we examined the possibility that the gravity waves responsible for the ionospheric rise and fall above Arecibo, were launched by the December 26, 2004 tsunamis as they propagated into the Atlantic Ocean [Titov et al., 2005]. Our GPS data recorded in Asia, Europe, and the Caribbean indicate that global TIDs were induced at the wake of tsunami-launched gravity waves. The possibility that seismic events can affect space weather halfway around the world on the following day raises challenges that merit further investigation.

3. Ionospheric Turbulence Generated by NAU-injected Radio Waves

Intense VLF whistler waves originating from radio transmitters or lightning discharges can interact with the ionosphere via the excitation of plasma instabilities. Lower hybrid waves and field-aligned zero-frequency plasma density irregularities can be parametrically excited in the ionosphere [Lee and Kuo, 1984]. The excited ionospheric density irregularities have scale sizes ranging from a fraction of 1 meter to 10 meters and align with geomagnetic field lines to form filaments [Labno et al., 2007]. The lower hybrid waves can accelerate electrons and ions along and across the geomagnetic field, respectively, generating non-Maxwellian distribution functions [Lynch et al.,1994] capable of exciting airglow. In fact, airglow effects were observed in coincidence with the operational cycles of a VLF transmitter [Chmyrev et al., 1976], and lower hybrid waves were detected over a powerful VLF transmitter [Berthelier et al., 1982; Bell et al., 1991]. The mechanism described by Lee and Kuo [1984] provides a basis for understanding the explosive spread F phenomena [Liao et al., 1989] and the spectral broadening of VLF waves during transionospheric propagation [Groves et al., 1988; Dalkir et al.,1992].

Experimental investigation of whistler wave interactions with ionospheric plasmas can be ideally conducted at Arecibo Observatory. A Naval transmitter code-named NAU is located nearby at Aguada, Puerto Rico, emitting radio waves at a power and frequency of 100 kW and 40.75 kHz, respectively. The Arecibo 430 MHz radar can be used to diagnose ionospheric plasma effects induced by NAU transmission-excited lower hybrid waves. A small fraction of NAU transmitted power, could be coupled into the ionosphere via refraction and mode conversion in the presence of ionospheric density irregularities. In this case large-scale field-aligned ionospheric irregularities act as waveguides to guide NAU signal to propagate along the Earth's magnetic field lines and facilitate the "linear mode conversion" of NAU signals into whistler waves. Only 50% of NAU signal power remains in the ionosphere after the "linear mode conversion" of the left-hand circularly polarized wave component into a whistler-mode wave" due to ionospheric plasma density gradients. Based on a simplified slab model of ionospheric plasmas, we obtained the transmission coefficient and, subsequently, estimate that ~7.5% of the incident NAU power can be coupled into the ionosphere at the altitude of F region.

The electric field amplitudes of NAU-generated 40.75 kHz whistler-mode waves in this case would reach 1 mV/m in the ionosphere. Such intense whistler-mode waves can parametrically excite lower hybrid waves and zero-frequency field-aligned density irregularities in ionospheric plasmas within a second [Lee and Kuo, 1984]. As mentioned before, the coupling of transmitted power to ionospheric plasmas can be enhanced in the presence of density irregularities. Thus, it is reasonable to speculate that NAU signals can be favorably coupled into ionospheric plasmas during the spread F events, which typically occurs as a nighttime phenomenon at Arecibo. Based on these expectations we conducted a series of Arecibo experiments between 20:00 and 24:00 local time (LT) during 20-27 December, 2004 to investigate ionospheric plasma interactions with NAU-

generated 40.75 kHz whistler-mode waves in the F region.

3.1. Plasma Line Enhancement in F region

Illustrated in Figure 13 is our experimental setup at the Arecibo Observatory, which is aimed at investigating interactions between NAU-generated 40.75 kHz whistler-mode waves and ionospheric F region plasmas. The 430 MHz radar was operated to take measurements of plasma lines, while a nearby ionosonde at Arecibo Observatory was used to monitor the occurrence of spread F irregularities. The distance from Arecibo Observatory to the NAU site is approximately 52 km. The magnetic dip angle over Arecibo is about 50°.
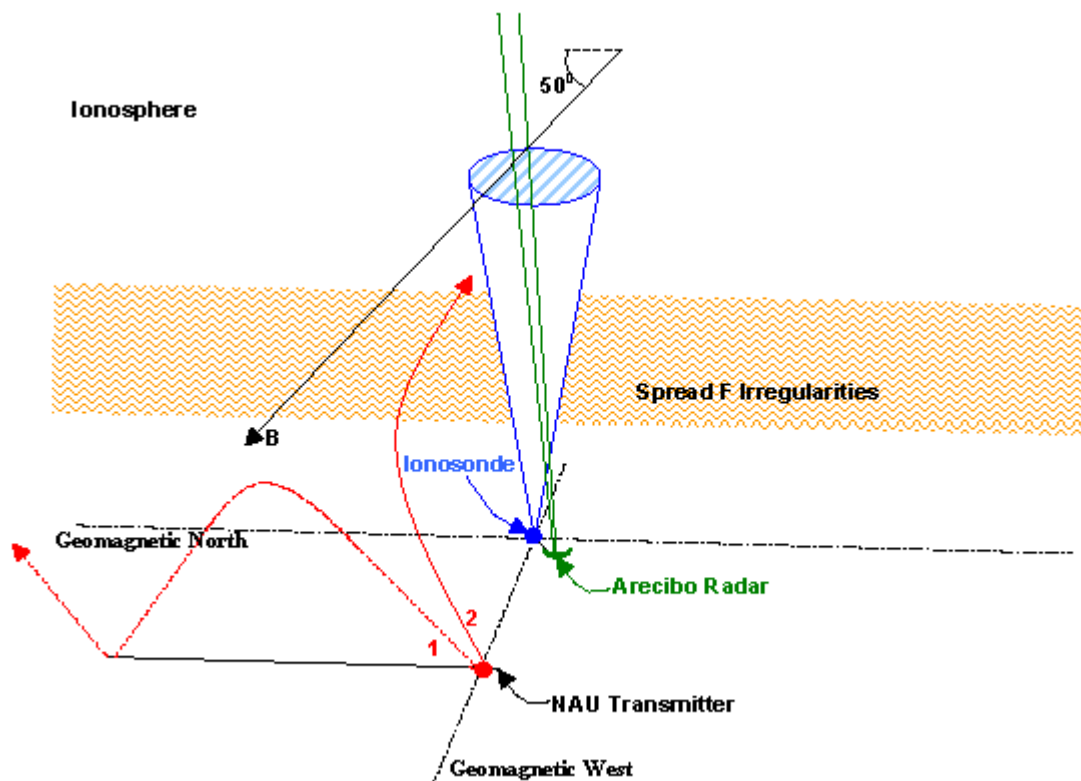

Figure 13. Illustration of experimental setup at Arecibo to investigate F-region plasma line enhancement caused by NAU-generated 40.75 kHz whistler waves. The 40.75 kHz signals emitted from NAU can propagate either as subionospheric waves (denoted by Ray 1) or whistler waves (denoted by Ray 2) in the ionosphere. The coupling of NAU signals into the ionosphere can be enhanced by ionospheric density irregularities.

During our experiments conducted from December 20 to December 27, 2004 between 20:00 and 24:00 LT, NAU transmissions were always recorded by our VLF/LF receiver.

The NAU signals propagated largely as subionospheric waves (denoted by Ray 1 in the figure) within the waveguide formed by the Earth's crust and the bottomside of the ionosphere. However, when these 40.75 kHz waves impinged upon the interface between the neutral atmosphere and the ionosphere, a small fraction of the transmitted power could have been coupled into the ionosphere via refraction and mode conversion. After entering the ionosphere, these 40.75 kHz signals propagated in the form of whistler-mode waves (denoted by Ray 2).

During our experiments spread F events occurred usually after 20:30 LT and persisted for several hours. The coupling of NAU-transmitted power to ionospheric plasmas was enhanced in the presence of spread F irregularities. The Arecibo radar transmitted vertically from the stationary linefeed throughout the experiments to take plasma line measurements, monitoring ionospheric plasma effects induced by the NAU-generated 40.75 kHz whistler-mode waves. Because of the nighttime environmental conditions, we could avoid getting photoelectron-induced plasma lines in experiments. The coded-long pulse technique was used to take plasma line measurements at altitudes from 90 to 495 km with a height resolution of 150 m. Frequency-upshifted radar return signals, corresponding to downgoing plasma waves, were recorded.

Presented in Figure 14 is one set of data, showing prominent plasma line enhancement in the F region, when the NAU transmitter was on and spread F echoes were intense, as monitored by our VLF/LF receiving system and Arecibo ionosonde, respectively. This data has three sequential frequency-altitude-intensity (FRI) plots of enhanced plasma lines taken at 00:22:21, 00:22:31, and 00:22:41 local time (LT), respectively, on December 21, 2004. The vertical axis marked by "power (A.U.)" denotes the relative backscatter power spectra of measured plasma lines on a linear scale. A.U. stands for arbitrary unit. Enhanced plasma lines occurred at 00:22:31 LT in the middle plots [denoted by (B) & (B')]. The FRI plot in Figure 14B is recast explicitly with a color bar in Figure 14B' to show the broad power spectrum of this prominent event. They appeared at altitudes around 300 ±70 km, having a signal to noise ratio (SNR) of ~ 70. The frequency spectra of these enhanced plasma lines range from 3.5 to 5 MHz with a center frequency around 4.2 MHz. Note that there was an interference associated with radio signals at 2.5 MHz from National Institute of Standard and Technology (NIST) recorded throughout the experiments. Each spectrum was generated with a 10-second integration time. Because no enhanced plasma lines were recorded 10 seconds earlier at 00:22:21 LT or 10 seconds later at 00:22:41 LT, the mechanism responsible for the observed F-region plasma line enhancement can be completed in less than 10 seconds.

27

F Region Plasma Line Enhancement
on December 21, 2004

00:22:21 LT (A)
00:22:31 LT (B and B')
00:22:41 LT (C)

Rescaled plot of the observed
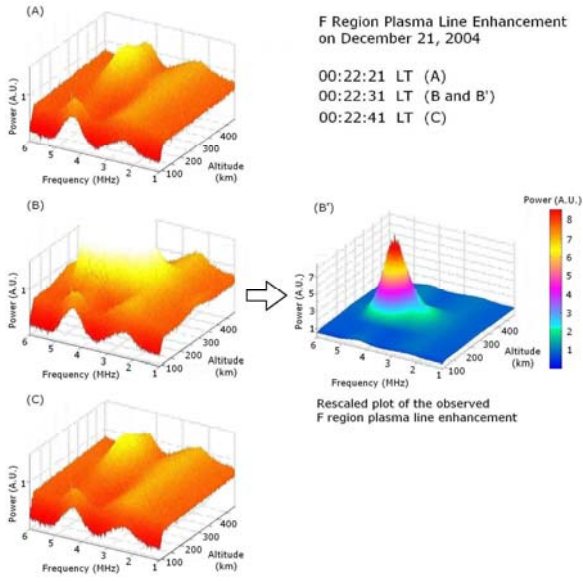F region plasma line enhancement

Figure 14. A set of data showing prominent F-region plasma line enhancement, recorded in the presence of spread F events, when NAU transmitter was on.

Another set of data is given in Figure 15, showing a less prominent but more commonly observed case of F-region plasma line enhancement. Displayed here are a sequence of three FRI plots, acquired at 20:49:07, 20:49:17, and 20:49:27 LT, respectively, on December 25, 2004.   This set of data shows sequentially the occurrence of F-region plasma line enhancement at 20:49:17 LT, and disappearance in less than 10 seconds. The enhanced plasma lines appeared at altitudes around 320 ±80 km, having a SNR of ~ 6, and a center frequency at 4 MHz with a bandwidth of ~ 1.5 MHz.   No F-region plasma line enhancement events were observed in the absence of spread F activities.

Plasma Line Enhancement on December 26, 2004

(A) 20:49:07 LT   (B) 20:49:17 LT   (C) 20:49:27 LT

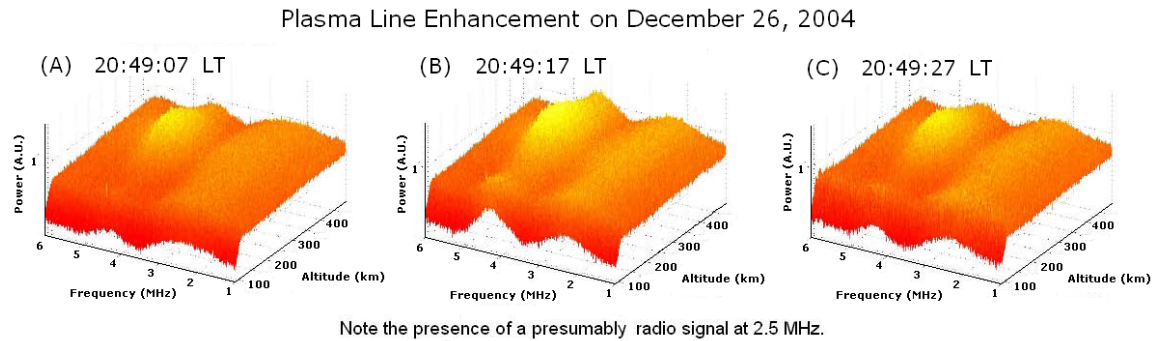Note the presence of a presumably radio signal at 2.5 MHz.

Figure 15.   A set of data showing less prominent but more commonly observed F-region plasma line enhancement in the presence of spread F events, when NAU transmitter was on.

3.2. A Source Mechanism

While there are not known mechanisms which can produce nighttime F region plasma line enhancement over Arecibo, we believe that the NAU-generated 40.75 kHz whistler-mode waves are the potential source responsible for it.   As elaborated below, the 40.75 kHz whistler-mode waves acting as the pump waves can excite lower hybrid waves in the F region plasmas, which subsequently accelerate electrons along the Earth's magnetic field.   The plasma waves associated with the streaming electrons were detected by the Arecibo backscatter radar beams as enhanced plasma lines. The spectral features of these measured plasma lines are shown to be consistent with this proposed source mechanism.

The NAU 40.75 kHz transmitter in Puerto Rico emits at 100 kW. Even if a few percent ($\sim$ 7.5% as estimated) of the radiated power couples into the ionosphere, the electric field amplitudes of the 40.75 kHz whistler-mode waves would reach 1 mV/m in the ionospheric F region.   Such intense whistler-mode waves can parametrically excite lower hybrid waves and zero-frequency field-aligned density irregularities by a four-wave interaction process [Lee and Kuo, 1984a], as delineated in Figure 16.
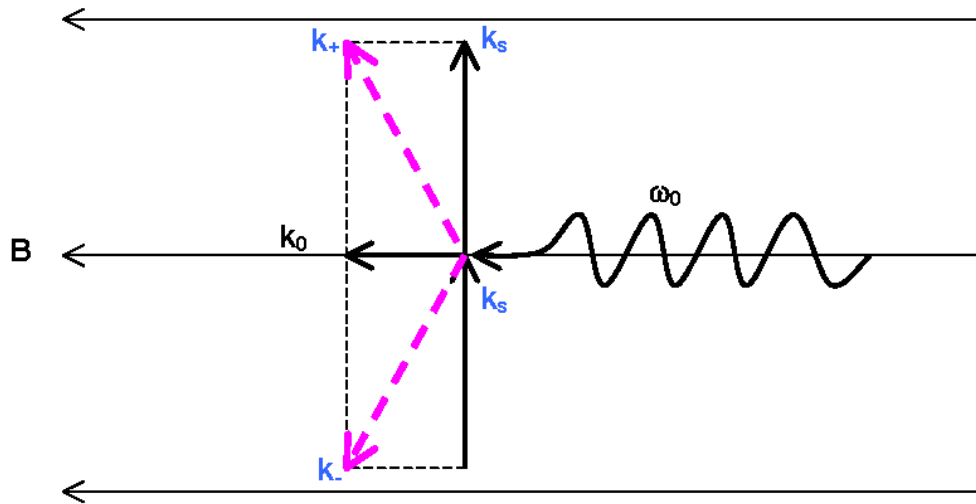

Figure 16.   A four-wave interaction process showing that 40.75 kHz whistler waves can parametrically excite Stokes and anti-Stokes lower hybrid waves together with zero-frequency field-aligned density irregularities.   The excited lower hybrid waves have a single frequency of 40.75 kHz with a spectrum of wavelength.

This whistler wave-plasma interaction process satisfies the following wave frequency and wave vector matching relations:

$\omega_o = \omega^+_{\ell h} - \omega_s$ [Eq. (1a)]

$\omega_o = \omega^-_{\ell h} + \omega^*_s$ [Eq. (1b)]

$k_o = k_+ - k_S$ [Eq. (2a)]

$k_o = k_- + k_S$ [Eq. (2b)]

where (ω_o, k_o) denotes the 40.75 kHz whistler-mode wave, that excites an "anti-Stokes" lower hybrid wave ($\omega^+_{\ell h}$, k_+), a "Stokes" lower hybrid wave ($\omega^-_{\ell h}$, k_-), together with a "zero-frequency" plasma mode (ω_s, k_S).   That is, the real component of $\omega_s = 0$ and the real component of $\omega^+_{\ell h}$ ($\omega^-_{\ell h}$) equals to ω_o. Here, ω^*_s is the complex conjugate of ω_s.

We adopt the following ionospheric plasma parameters: $\omega_o/2\pi = 40.75$ kHz, $\omega_{pe}/2\pi = 4$ MHz, $\omega_{ce}/2\pi = 1.0$ MHz and assume that the whistler-mode waves propagate along the Earth's magnetic field, with a wave normal angle $\psi = 0$, to simplify the analysis of this physical process.   Then, the wavelength of 40.75 kHz whistler-mode waves is found to be ~ 375 m from the following whistler dispersion relation (Eq. (3)).

$(ck_o/\omega_o)^2 \approx \omega_{pe}^2/(\omega_o \omega_{ce})$ [Eq. (3)]

The dispersion relation for lower hybrid wave ($\omega_{\ell h}$, $k_{\ell h}$) is given by

$\omega_{\ell h} = \omega_{\ell hR} [1 + (k_{\ell h \parallel}^2 M_i / k_{\ell h \perp}^2 m_e)]^{\frac{1}{2}}$ [Eq. (4)]

where $\omega_{\ell h} = \omega_o$; $\omega_{\ell hR} = \omega_{pi} / [1 + (\omega_{pe} / \omega_{ce})^2]^{\frac{1}{2}} \approx 35.8$ rad-kHz is the lower hybrid resonance frequency, m_e the electron mass, M_i ($= 1840$ x 16 m_e) the atomic oxygen ion mass, ω_{pi} the atomic oxygen ion plasma frequency, ω_{ci} the atomic oxygen ion gyro-frequency, and $k_{\ell h \parallel}$ and $k_{\ell h \perp}$ are the parallel and perpendicular components of the lower hybrid wave vector, respectively.

One can notice from Eq. (4) that lower hybrid waves excited by the 40.75 kHz whistler-mode waves have the same frequency ($\omega_{\ell h} = \omega_o$), but with a continuous spectrum of wave vectors. We should point out at this moment that the instability mechanism of Lee and Kuo [1984a] is different from the mode conversion of whistler mode waves to lower hybrid mode with much less intensities by scattering from ionospheric density irregularities [Bell and Ngo, 1990; Groves et al., 1988].   The instability mechanism and the mode conversion process can contribute additively to the spectral broadening of VLF waves in the topside of the ionosphere [Bell and Ngo, 1990; Groves et al., 1988].

We examine how the lower hybrid waves excited by the 40.75 kHz whistler-mode waves can accelerate electrons along the Earth's magnetic field and yield the detected plasma lines in F region as follows. The Arecibo 430 MHz radar detects plasma modes with a wavelength of 34 cm which is half of the radar wavelength of 68 cm, following the Bragg scattering condition. The radar-detected F-region plasma lines have a center frequency

around 4 MHz with a bandwidth of 1.5 MHz. Hence, the phase velocities of those waves associated with the streaming electrons range from 1.1 x10^6 to 1.6 x10^6 m/s. Then, the inferred phase energies of those streaming particles have a range of 7.2 -15 eV.

Under the resonant interaction condition, the lower hybrid waves accelerating these electrons have the same range of parallel phase velocities ($f_{\ell h} \lambda_{\ell h \parallel}$) from 1.1 x10^6 to 1.6 x10^6 m/s, where $f_{\ell h}$ and $\lambda_{\ell h \parallel}$ represent the frequency and parallel wavelength of lower hybrid waves, respectively. Because these lower hybrid waves have a single frequency of 40.75 kHz, they have a spectrum of parallel wavelength ($\lambda_{\ell h \parallel}$) ranging, at least, from 26.8 to 39.2 m. The corresponding perpendicular wavelengths ($\lambda_{\ell h \perp}$) of these lower hybrid waves, calculated from Eq. (4), have magnitudes from 1.1 to 1.6 m. In other words, electrons in F region are energized by meter-scale lower hybrid waves excited by the NAU-generated whistler-mode waves.

3.3. Summary and Conclusions

We propose that the Naval transmitter (NAU) is responsible for causing the enhanced plasma lines, detected by Arecibo 430 MHz radar in the nighttime ionosphere F region, in the presence of spread F events.   The NAU-generated 40.75 kHz whistler-mode waves are intense enough to excite lower hybrid waves and zero-frequency field-aligned plasma density irregularities in the ionosphere over Arecibo. These lower hybrid waves, generated in a broad range of altitude at the wake of 40.75 kHz whistler-mode waves, have a single frequency of 40.75 kHz with a spectrum of wavelengths. They can effectively accelerate electrons continuously along the Earth's magnetic field with energies from a fraction of 1 eV to 10 eV.   These energetic streaming electrons, when detected by Arecibo 430 MHz radar, give rise to enhanced plasma lines with a frequency spectrum of ~ 3.25 – 4.75 MHz.

4. Personnel for Reported Research

The reported research work was carried out by the Principal Investigator: M.C. Lee with his graduate students: R. Pradipta, J.A. Cohen, D.L. Rokusek and undergraduate students: S.E. Dorfman, L.M. Burton and A. Labno. R. Pradipta and D.L. Rokusek have accomplished their M.S. theses under the support of this grant.

References

Artru J., P. Lognonné et E. Blanc (2001), Normal modes modeling of post-seismic ionospheric oscillations, Geophysical Res. Lett., 28, 697.

Artru, J., T. Farges, P. Lognonné (2004), Acoustic waves generated from seismic surface

waves: propagation properties determined from Doppler sounding observation and normal-modes modeling. Geophys. J. Int., 158, 1067.

Artru, J., V. Ducic, H. Kanamori, P. Lognonne, and M. Murakami (2005a), Ionospheric detection of gravity waves induced by tsunamis, Geophys. J. Int, 160, 840.

Artru, J., P. Lognonné, G. Occhipinti, F. Crespon, R. Garcia, E. Jeansou and M. Murakami (2005b), Tsunami detection in the ionosphere, Space Research Today, 163, 24-27.

Basu, B. (1997), Generalized Rayleigh-Taylor instability in the presence of time-dependent equilibrium, J. Geophys. Res., 102, 17,305.

Basu, Su., Sa. Basu, S. Ganguly, and J. A. Klobuchar (1981), Generation of kilometer scale irregularities during the midnight collapse at Arecibo, J. Geophys. Res., 86, 7607.

Behnke, R. A. (1979), F layer height bands in the nocturnal ionosphere over Arecibo, J. Geophys. Res., 84, 974.

Bell, T.F. and H.D. Ngo, Electrostatic lower hybrid waves excited by electromagnetic whistler mode waves scattering from planar magnetic-field-aligned plasma density irregularities, J. Geophys. Res., 95, 149 1990.

Bell, T.F., U.S. Inan, V.S.Sonwalker, and R.A. Helliwell, DE-1 observations of lower Hybrid waves excited by VLF whistler mode waves, Geophys. Res. Lett., 18, 393, 1991.

Berthelier, J.J. et al., Measurements of the VLF electric and magnetic components of waves and DC electric field on board the AUREOL-3 spacecraft: The TBF-ONCH experiments, Ann. Geophys., 38, 643, 1982.

Bishop R. L., N. Aponte, G. D. Earle, M. Sulzer, M. F. Larsen, G. S. Peng (2006), Arecibo observations of ionospheric perturbations associated with the passage of Tropical Storm Odette, J. Geophys. Res., 111, A11320, doi:10.1029/2006JA011668.

Booker, H. G. and H. W. Wells (1938), Scattering of radio waves by the F region of the ionosphere, J. Geophys. Res., 43, 249.

Chmyrev, V.M., V.K. Roldugin, I.A. Zhulin, M.M. Mogilevskii, V.I. Di, V.K. Koshelevskii, V.A. Bushmarin, and O.M. Raspopov, Artificial injection of very low frequency wave into the ionosphere and the magnetosphere of the earth, JETP Lett., 23,49, 1976.

Dalkir, Y.R., M.C. Lee, K.M. Groves, and S.P. Kuo, A mechanism responsible for the

observation of symmetric lower hybrid sidebands and a low frequency mode in the upper ionosphere, J. Geophys. Res., 97, 17995, 1992.

Davis, M. J., and A. V. da Rosa (1969), Traveling ionospheric disturbances originating in the auroral oval during polar substorms, J. Geophys. Res., 74, 5,721.

DasGupta, A., A. Das, D. Hui, K. K. Bandyopadhyay, and M. R. Sivaraman (2006), Ionospheric perturbation observed by the GPS following the December 26th, 2004 Sumatra-Andaman earthquake, Earth Planets Space, 35, 929 – 959.

Djuth, F.T., M.P. Sulzer, J.H. Elder, and V. B. Wickwar (1997), High-resolution studies of atmosphere-ionosphere coupling at Arecibo Observatory, Puerto Rico, Radio Sci., 32, 2321–2344.

Djuth, F.T., M.P. Sulzer, S.A. Gonzales, J.D. Mathews, J.H. Elder, and R.L. Walterscheid (2004), A continuum of gravity waves in the Arecibo thermosphere?, Geophys. Res. Lett., 31, 10.1029/2003GL019376.

Ducic, V., J. Artru and P. Lognonné (2003), Ionospheric remote sensing of the Denali Earthquake Rayleigh surface waves, Geophys. Res. Lett., 30, 1951, doi:10.1029/2003GL017812.

Eccles, J. V. (1998), A simple model of low-latitude electric fields, J. Geophys. Res., 103, 26,699.

Francis, S. H. (1973), Acoustic-gravity modes and large-scale traveling ionospheric disturbances of a realistic, dissipative atmosphere, J. Geophys. Res., 78, 2278, 1973.

Garcia, R., F. Crespon, and P. Lognonne (2005), Observations of post-seismic ionospheric disturbances following the great Sumatra earthquake from GPS networks, Geophys. Res. Abs., 7, 03186.

Groves, K.M., M.C. Lee, and S.P. Kuo, Spectral broadening of VLF radio signals traversing the ionosphere, J .Geophys. Res., 93, 14683, 1988.

Hao, Y-Q., Z. Xiao, D-H. Zhang (2006), Responses of the Ionosphere to the Great Sumatra Earthquake and Volcanic Eruption of Pinatubo, Chinese Phys. Lett., 23, 1955-1957.

Hines, C. O. (1960), Internal atmospheric gravity waves at ionospheric heights, Can. J. Phys., 38, 1441-1481, 1960.

Hines, C. O. (1965), Motions of the neutral atmosphere, in Physics of the Earth's Upper Atmosphere, edited by C.O. Hines, I. Paghis, T.R. Hartz, and J.A. Fejer, pp. 134-156,

Prentice-Hall, Englewood Cliffs, N.J.

Huang, C. Y., W. J. Burke, J. S. Machuzak, L. C. Gentile, and P. J. Sultan (2001), DMSP observations of in the topside ionosphere near solar maximum, J. Geophys. Res., 106, 8,131.

Kelley, M. C., and M. F. Larsen (1981), Gravity wave initiation of equatorial spread F; A case study, J. Geophys. Res., 86, 9,087.

Kelley, M. C., C. E. Seyler, and S. Zargham (1987), Collisional interchange instability 2. A comparison of the numerical simulations with the in situ experimental data, J. Geophys. Res., 92, 10073.

Komjathy, A., B. Iijima, L. Sparks , and A. Mannucci, Detecting Ionospheric-seismic signatures during the Sumatra earthquake event using ground and space-borne GPS measurements, presented at National Radio Science Meeting, Boulder, Colorado, January 4-7, 2006.

Labno, A., R. Pradipta, M. C. Lee, M. P. Sulzer, L. M. Burton, J. A. Cohen, S. P. Kuo, and D. L. Rokusek (2007), Whistlermode wave interactions with ionospheric plasmas over Arecibo, J. Geophys. Res., 112, A03306, doi:10.1029/2006JA012089.

Lee, M.C., and S.P. Kuo, Production of lower hybrid waves and field-aligned plasma density striations by whistlers, J. Geophys. Res., 89, 10873, 1984.

Lee, M. C., R. J. Riddolls, W. J. Burke, M. P. Sulzer, E. M. C. Klien, M. J. Rowlands, and S. P. Kuo (1998a), Ionospheric plasma bubble generated by Arecibo heater, Geophys. Res. Lett., 25,579.

Lee, M. C., R. J. Riddolls, W. J. Burke, M. P. Sulzer, S. P. Kuo, and E. M. C. Klien (1998b), Generation of large sheet-like ionospheric plasma irregularities at Arecibo, Geophys. Res. Lett., 25, 579

Lee, M. C., E. M. C. Klien, W. J. Burke, A. X. Zhang, R. J. Riddolls, S. P. Kuo, M. P. Sulzer, and B. Isham (1999), Augmentation of natural ionospheric plasma turbulence by HF heater waves, Geophys. Res. Lett., 26, 37.

Lee, M. C., R. Pradipta, W. J. Burke, A. Labno, L. M. Burton, J. A. Cohen, S. E. Dorfman, A. J. Coster, M. P. Sulzer, and S. P. Kuo (2008), Did Tsunami-Launched Gravity Waves Trigger Ionospheric Turbulence over Arecibo?, J. Geophys. Res., 113, A01302, doi:10.1029/2007JA012615.

Liao, C.P., J.P. Freidberg, and M.C. Lee, Explosive spread F caused by lightning-induced

Electromagnetic effects, J. Atmos. Terr. Phys., 51, 751, 1989.

Liu J.-Y., Y.-B. Tsai, K.-F. Ma, Y.-I. Chen, H.-F. Tsai, C.-H. Lin, M. Kamogawa, C.-P. Lee, Ionospheric GPS total electron content (TEC) disturbances triggered by the 26 December 2004 Indian Ocean tsunami, J. Geophys. Res., 111, 1029, 2006.

Lognonné, P., C. Clévédé and H. Kanamori (1998), Normal mode summation of seismograms and barograms in an spherical Earth with realistic atmosphere, Geophys. J. Int., 135, 388-406.

Lognonné, P., E. Jeansou, R. Garcia, J. Artru, G. Occhipinti, F. Crespon, J. Achache, J. Helbert, and G. Moreaux (2005), Detection of the Ionospheric perturbation associated to the tsunami of December 26th, 2004 with TOPEX and Jason-1 TEC data, Geophys. Res. Abs., 7, 09028.

Lognonné, P. Juliette Artru, Raphael Garcia, François Crespon, Vesna Ducic, Eric Jeansou, Giovani Occhipinti, Jérome Helbert, Guilhelm Moreaux, Pierre-Emmanuel Godet (2006), Ground based GPS tomography of ionospheric post-seismic signal., Planet. Space. Science, 54, 528540.

Lynch, K.A., R.L. Arnoldy, P.M. Kintner, and J.L. Vago, Electron distribution function Behavior during localized transverse ion acceleration events in the topside auroral zone, J. Geophys. Res., 99, 2227, 1994.

McClure, J. P., S. Singh, D. K. Bamgboye, F. S. Johnson, and H. Kil (1998), Occurrence of equatorial F region irregularities: Evidence for tropospheric seeding, J. Geophys. Res., 103, 29,119.

Meriwether, J. W., J. L. Mirick, M. A. Biodi, F. A. Herero, and C. G. Fesen (1996), Evidence for orographic wave heating in the equatorial thermosphere at solar maximum, Geophys. Res. Lett., 23, 2177.

Nicolls, M. J., M. C. Kelley, A. J. Coster, S. A. González, and J. J. Makela (2004), Imaging the structure of a large-scale TID using ISR and TEC data, Geophys. Res. Lett., 31,1029.

Nicolls, M.J. and M.C. Kelley (2005), Strong evidence for gravity wave seeding of an ionospheric plasma instability, Geophys. Res. Lett., 32, 679.

Occhipinti, G., P. Lognonné, E.Kherani, H.Hébert (2006), 3D Waveform modeling of ionospheric signature induced by the 2004 Sumatra tsunami, 33, L20104, doi : 10.1029/2006GL026865, Geophys Res. Lett.

Occhipinti, G., Observations multi-paramètres et modélisation de la signature

ionosphérique du grand séisme de Sumatra, Ph.D. thesis. Institut de Physique du Globe de Paris. December 2006.

Ossakow, S. L. (1981), Spread-F theories: A review, J. Atmos. Terr. Phys., 43, 437.

Rich, F. J., and M. Hairston (1994), Large-scale convection patterns observed by DMSP, J. Geophys. Res., 99, 3827.

Rideout, W. and A. Coster (2006), Automated GPS processing for global total electron content data GPS Solut (2006) DOI 10.1007/s10291-006-0029-5.

Sentman, D. D.,E.M.Wescott, R. H. Picard,J. R.Winick, H. C. Stenbaek-Nielsen, E.M.Dewan, D.R. Moudry, F. T. Sao Sabbas, M. J. Heavner, and J. Morrill (2003), Simultaneous observations of mesospheric gravity waves and sprites generated by a midwestern thunderstorm, J. Atmos. Solar Terres. Phys., 65,5.

Singh, S., F. S. Johnson, and R. A. Power (1997), Gravity wave seeding of equatorial plasma bubbles, J. Geophys. Res., 102, 7399.

Stevenson, D. (2005), Tsunami and earthquakes: What physics is interesting?, Phys. Today, 58, 10.

Sultan, P. J. (1996), Linear theory and modeling of the Rayleigh-Taylor instability leading to the occurrence of equatorial spread F, J. Geophys. Res., 101, 26,875.

Titov, V., A. B. Rabinovich, H. O. Mofjeld, R. E. Thomson, and R. I. Gonzalez (2005), The global reach of the 26 December 2004 Sumatra tsunami, Science, 309, 2045-2048.

Tsunoda, R. T., R. C. Livingston, J. P. McClure, and W. B. Hanson (1982), Equatorial plasma bubbles: Vertically elongated wedges from the bottomside F layer, J. Geophys. Res., 87, 9171.

Wilson, M. (2005), Modeling the Sumatra-Andaman earthquake reveals a complex, nonuniform rupture, Wilson, M., Modeling the Sumatra-Andaman earthquake reveals a complex, nonuniform rupture, Phys. Today, 58, 19.

Zalesak, S. T., and S. L. Ossakow (1982), On the prospect for artificially inducing equatorial spread F, Memo. Rep. 4899, Nav. Res. Lab., Washington, D.C.